Chemical Physics 158 (1991) 421–446
North-Holland

Coupling of protein motion to electron transfer: molecular dynamics and stochastic quantum mechanics study of photosynthetic reaction centers

Klaus Schulten and Markus Tesch
Beckman Institute and Department of Physics, University of Illinois, Urbana, IL 61801, USA

Received 25 July 1991

We investigate how electron transfer is controlled by protein motion in photosynthetic reaction centers. Our study is based on molecular dynamics (MD) simulations of two electron transfer steps in the reaction center of *Rps. viridis* at physiological and at lower temperatures. The classical simulations of protein nuclear motions are complemented by a quantum mechanical description for the electron transfer, incorporating in a two-state model a coupling to the classical protein motion through a fluctuating diagonal contribution which is determined as the energy difference $\Delta E(t)$ between reactant and product states at each instance of time. The properties of $\Delta E(t)$, the distribution $p(\Delta E)$ and correlation function $\langle \Delta E(t+\tau)\Delta E(\tau)\rangle$, are investigated and a stochastic quantum mechanical model for electron transfer is introduced that incorporates three characteristics of $\Delta E(t)$, namely its mean value, its rms-deviations from the mean, and the mean relaxation time of its correlation function. The calculations which go beyond second-order perturbation theory predict a bell-shaped dependence of the electron transfer rate on redox energies with a so-called inverted region and with a width of about 20 kcal/mol (about 10 kcal/mol for the stochastic model). Rapid (0.05 ps) dielectric relaxation after electron transfer induces a shift of the mean $\langle \Delta E\rangle$ which causes reactant and product states to become sufficiently out of resonance and which, thereby, prevents electron back-transfer. It is shown that all components of photosynthetic reaction centers contribute rather evenly to the coupling between electron transfer and medium.

1. Introduction

1.1. Properties of photosynthetic reaction centers

Within photosynthetic organisms, membrane-bound protein-pigment complexes – the photosynthetic reaction centers – perform the primary process of photosynthesis, the transformation of light energy into an electrical membrane potential. In a reaction center, energy conversion is initiated by photo-excitation of a primary donor followed by electron transfer steps which yield a pair of negative and positive charges separated across the width of a cell membrane (for reviews see refs. [1–3]). Reaction centers of purple photosynthetic bacteria of *Rb. sphaeroides* [4–6] and *Rps. viridis* [7–9], whose structures are available at high resolution, provide ideal systems to study photo-induced charge separation. For the reaction center of *Rps. viridis*, the cofactors involved in the conduction of the photo-excited electron and the electron transfer kinetics [1,2,10] are depicted in fig. 1. A photon excites a bacteriochlorophyl dimer, the so-called *special pair* (P_S), which then rapidly transfers an electron to a bacteriopheophytin H_L, possibly via bacteriochlorophyl B_L [11,12]. In a second step, an electron is transferred to a menaquinone Q_A (a ubiquinone in *Rb. sphaeroides*) and, in a third step, to a ubiquinone Q_B. This electron transfer chain is optimized to achieve a high quantum yield, i.e., absorption of a photon results with very high probability in the reduction of Q_B [13]. This chain is optimized also for high energy efficiency, although to a lesser degree than for high quantum yield [14].

An essential feature of electron transfer in the photosynthetic reaction centers is its peculiar temperature dependence. Fleming et al. [15] measured the rate of the electron transfer $P_S \rightarrow H_L$ as they lowered the temper-

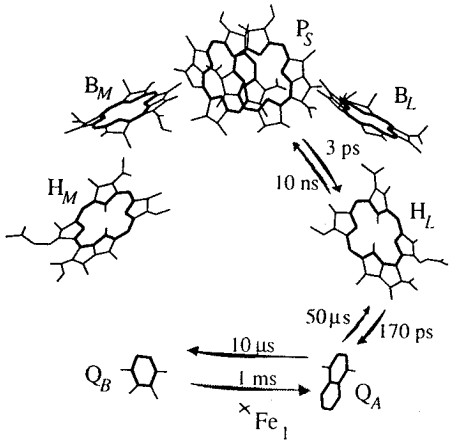

Fig. 1. Cofactors of the reaction center of *Rps. viridis* without their side chains. Electron transfer times at 300 K are given for both forward and backward directions. Central ring atoms involved in bonds drawn by thick lines will be used below to determine structural properties of cofactors. The chromophores B_M and H_M of the so-called "non-functional branch" do not participate in the electron transfer processes.

ature from 300 down to 8 K, and found the electron transfer rates to increase in both reaction centers. At 8 K, the rate in *Rps. viridis* is a factor of four larger than the rate at room temperature; in *Rb. sphaeroides* the rate is twice as large. Kirmaier and Holten [16] determined the rates for the electron transfer $H_L \rightarrow Q_A$. The rate is temperature-independent in *Rps. viridis*; in *Rb. sphaeroides*, the rate at 5 K is three times larger than the rate at room temperature.

Of interest is also the dependence of transfer rates on the redox energies of donor–acceptor pairs involved in the transfer chain. Two experiments show how electron transfer rates change when the redox energies of the donor–acceptor pair are altered. Kirmaier et al. [17] replaced the native H_L by a bacteriochlorophyl, a replacement which changed the redox energy by about 0.1 eV. Such genetically engineered reaction centers show the following behavior: (1) the electron transfer $P_S \rightarrow H_L$ is slowed down insignificantly; (2) the quantum yield for $P_S^+ H_L^-$ formation is the same as for the wild type reaction center; (3) the charge recombination to the ground state is about ten times faster than in the wild-type reaction center; (4) the reduction of Q_A is about three times slower than in the wild type; and (5) as a result of (3) and (4) the quantum yield for $P_S^+ Q_A^-$ formation decreases to about 60%. In another set of experiments investigating the transfer $H_L \rightarrow Q_A$, Gunner and Dutton [18] replaced the menaquinone Q_A by other quinones, varying the redox energies in a range of about 0.4 eV. These authors observed a rather weak dependence of the rate on temperature and redox energy.

1.2. Previous simulations

The availability of high-resolution structures allows investigations of photosynthetic reaction centers at a molecular level. For example, by molecular dynamics (MD) simulations Treutlein et al. [14] and Creighton et al. [19] simulated the dynamics of the primary charge separation process. Warshel et al. [20] calculated the temperature dependence of the rate for the transition $H_L^- Q_A \rightleftharpoons H_L Q_A^-$ by "dispersed polaron" simulations assuming that the characteristics of the system, i.e., structure and free energy envelope, are independent of temperature. In the present paper, we extend these studies and examine systematically the role of the thermal motion of the atoms in the photosynthetic reaction center of *Rps. viridis* on the electron transfers $P_S \rightarrow H_L$ and $H_L \rightarrow Q_A$.

1.3. Similarity to electron transfer in liquids

We like to emphatically suggest that our study is not only relevant for biological redox processes, but actually for any electron transfer process in organic media which have recently received much attention in a variety of studies [21–24]. The reason is that the photosynthetic reaction center, in many respects, behaves like an organic

liquid in that the bulk of its atoms are coupled through their partial charges and through long-range Coulomb forces to its redox processes. This "liquid", however, has a particular (and well-known) structure which bears the important advantage that it can serve as a proper starting point for MD simulations. The covalent bonding of the protein, deviant from properties of real liquids, does not affect very much the dynamics on the time scales relevant to the primary electron transfer processes in photosynthetic reaction centers.

One may criticize that MD simulations are based on artificial force fields and that quantitative agreement with the real system is limited. We like to claim that even if this critique to some degree applies, the simulated protein system provides an interesting medium and electron transfer system in its own right, one for which every detail is under numerical control, and understanding electron transfer in a simulated protein should be of nearly as much interest as understanding electron transfer of, say, pyrene-dimethylaniline in methanol. A reason is that the effect of the environment on electron transfer is transmitted between medium and donor–acceptor system through Coulomb forces, which are actually rather faithfully presented in simulations. The simulations can shed light on some essential aspects of electron transfer theories which, so far, have been largely phenomenological in that they provide a microscopic description for some of the properties employed in these theories. Prime examples, in this respect, are the so-called solvent polarization coordinate and the "diffusion constant" describing Brownian motion along this coordinate as introduced, for example, by Sumi and Marcus [25].

1.4. Spin–boson formulation of electron transfer–medium coupling

The present paper can be considered only a first step towards understanding the coupling between medium and electron transfer in the photosynthetic reaction center since we treat the atomic motion of the reaction medium classically, a treatment which is valid only in the high-temperature limit – a limit which, most likely, applies rather well at physiological temperatures at which the protein carries out its biological function. In an accompanying paper [26] we investigate the role of quantum effects of the protein nuclear motion and show that these effects indeed play a small role at $T=300$ K.

The simulations presented below suggest that the role of atomic motion of the medium (protein) on electron transfer can be cast in the form of the approximate Hamiltonian

$$\mathscr{H}'(\Delta E(t))+\sum_{\alpha}\left(\frac{p_\alpha^2}{2m}+\frac{1}{2}m\omega_\alpha^2(q_\alpha-q_{0\alpha})^2\right). \tag{1}$$

Here, $\mathscr{H}'$ describes a Hamiltonian which governs the electron transfer. This Hamiltonian depends on the energy difference ΔE between reactant and product electronic states which is given by

$$\Delta E(t)=\Delta E_0+\sum_{\alpha} c_\alpha(q_\alpha(t)-q_{0\alpha})\,. \tag{2}$$

The simplest form of the Hamiltonian $\mathscr{H}'$ is that of a two-state operator expressed in terms of the Pauli matrices σ_1 and σ_3

$$\mathscr{H}'=V\sigma_1+\frac{\epsilon}{2}\sigma_3-\frac{\Delta E(t)}{2}\sigma_3\,, \tag{3}$$

where V describes the electronic coupling and ϵ can be interpreted as a redox energy. The second term in the Hamiltonian describes an ensemble of independent oscillators which are coupled to the electron transfer (approximately) linearly through $\Delta E(t)$, i.e., displacements of the oscillators alter the energy difference between reactant and product states. The oscillators which represent vibrational and librational motions may be subject to frictional forces as described in ref. [27]. The frequencies ω_α which contribute to eq. (1) are of the order of 10–100 ps^{-1}. Eqs. (1–3) define the so-called spin–boson problem of quantum mechanics which has been studied exhaustively in ref. [28]. A similar Hamiltonian has been investigated by Onuchic [29]. The Hamiltonian in ref. [29] differed from eqs. (1–3) in that the author incorporated a dependence of the equilibrium position

$q_{0\alpha}$ on the electronic state replacing $q_{0\alpha}$ by $q_{0\alpha}\sigma_3$. In the spirit of the Born–Oppenheimer approximation we adopt in our simulations the view that the medium is too inert that even though, in principle, it is coupled to the electronic state, the medium cannot adapt to virtual transfers, like electron tunneling. Hence, we consider only Hamiltonians which are either in the reactant form, like eq. (1), or in the product form, like eq. (5) below. An adaptation of the medium to momentaneous electronic states in terms of a centroid approximation (for the electron part) in the framework of a path integral description has been developed and investigated in refs. [30,31].

In the limit $kT \gg \hbar\omega_\alpha$, $\forall\alpha$, the ensemble of oscillators can be described classically and $\Delta E(t)$ can be obtained from a classical simulation of the atomic motion of the medium. The properties of such $\Delta E(t)$ will be investigated below. The Fourier spectrum $\Delta\hat{E}(\omega)$ of $\Delta E(t)$ reveals the distribution of frequencies ω_α since, according to eq. (2), the spectrum can be written

$$\Delta\hat{E}(\omega) = \sum_\alpha c_\alpha A_\alpha \delta(\omega - \omega_\alpha) , \tag{4}$$

where A_α are the respective vibrational amplitudes, the thermal average of which measures classically $\sqrt{2kT/m\omega_\alpha^2}$. Our simulations below determine $\Delta\hat{E}(\omega)$ and, thereby, allow one to estimate the distribution of frequencies ω_α. One can then estimate very roughly the low-temperature behavior assuming zero point vibrations of the oscillators in eq. (1). The zero point vibrations, even at very low temperature, give rise to a (static) distribution of $\Delta E(t)$ values. This indicates that the medium in a quantum mechanical description will sustain an effect on electron transfer at low temperatures at which classical simulations yield vanishing amplitudes A_α and, hence, vanishing coupling. To appreciate this argument one should note that the long range of the Coulomb force couples essentially all atomic partial charges to electron transfer, such that the combined effect of zero point vibrations can be significant. Counteracting in this respect are, however, cancellations of the coupling due to charge neutralization. Our simulations below reveal, however, that despite such cancellations a coupling $\Delta E(t)$ remains which increases significantly with the volume of the medium.

A quantum mechanical calculation based on a spectral function $J(\omega) = \frac{1}{2}\pi\sum_\alpha (C_\alpha^2/m_\alpha\omega_\alpha)\delta(\omega - \omega_\alpha)$ which reproduces the key characteristics of our classical simulation, i.e., the distribution $p(\Delta E)$ and the relaxation time of the correlation function $\langle \Delta E(t)\Delta E(0)\rangle$, has been completed recently [26].

In the accompanying paper [26] we will employ the spin–boson model and evaluate the ensuing electron transfer rates in the temperature range 0–300 K to demonstrate the effects of zero point vibrations and the deviation from classical behavior.

1.5. Spin–boson model and dielectric response to electron transfer

At this point we may paraphrase, in the framework of the Hamiltonian (1), another essential result of this paper, namely, that electron transfer in the photosynthetic reaction center is followed by a very rapid (0.05 ps) dielectric relaxation of the medium. This relaxation corresponds to a change of the equilibrium positions $q_{0\alpha}$ of the oscillators in eq. (1), i.e., after the transfer the Hamiltonian is

$$\mathcal{H}' = \left(\Delta E_0 + \sum_\alpha c_\alpha (q_\alpha - q'_{0\alpha})\right) + \sum_\alpha \left(\frac{1}{2} m\omega_\alpha^2 (q_\alpha - q'_{0\alpha})^2 + \frac{p_\alpha^2}{2m}\right). \tag{5}$$

This description can be interpreted quite literally: the long-range Coulomb interaction exerts an influence on the medium after electron transfer, shifting the equilibrium positions of modes ($q_{0\alpha} \to q'_{0\alpha}$) slightly and rapidly. A suggestion to this effect had been made by Onsager [32]. A corrollary of this description is that the relaxation should proceed very rapidly in the bulk, and proceed even at very low temperatures, since small shifts $q_{0\alpha} \to q'_{0\alpha}$ do not create barriers and involve equilibration times of only a few vibrational periods. Such behavior is born out of our MD simulations presented below. Our simulations provide a molecular description of the

dielectric relaxation and, hence, complement earlier studies on continuum models. The need for such descriptions had been advocated, for example, in ref. [24].

1.6. Relationship of spin–boson model to Marcus theory of electron transfer

We like to draw finally the analogy between the description of electron transfer in terms of the Hamiltonians (1,5) and the existing theories of electron transfer. The analogy is actually very close and can be drawn using the well-known [33,34] Marcus free energy diagram depicted in fig. 2. In drawing this diagram one assumes that the energies of reactant and product states depend on a solvent polarization coordinate q in the form

$$E_R(q)=\tfrac{1}{2}fq^2, \quad E_P=\tfrac{1}{2}f(q-q_P)^2-\epsilon_0\,, \tag{6}$$

where q encompasses the nuclear configurations and, hence, the polarization of the medium (we disregard presently intramolecular degrees of freedom).

The medium undergoes thermal fluctuations which correspond to a Brownian motion along the medium polarization coordinate in fig. 2, described by a time series of $q(t)$ values. An approach based on such a description has been investigated in refs. [25,35]. The quantity in fig. 2 which controls the quantum mechanical transition between reactant and product states is the energy difference $\Delta E(t)=E_R[q(t)]-E_P[q(t)]$ which can be expressed

$$\Delta E(t)=fq_Pq(t)+\epsilon_0-\tfrac{1}{2}fq_P^2\,, \tag{7}$$

i.e., as a linear function of the medium polarization coordinate.

Before transfer the time series $q(t)$ is distributed according to the Boltzmann weight $p(q)=\exp[-E_R(q)/kT]$, and after transfer according to $p(q)=\exp[-E_P(q)/kT]$. According to eq. (7) $\Delta E(t)$ is then Gaussian-distributed, however, with different distributions before and after the transfer. Our simulations below reproduce such behavior for $\Delta E(t)$. The Gaussian shape is actually to be expected in a protein or any other large system, namely, as argued in ref. [36] due to the central limit theorem. The simulations allow one to state then that the potentials $E_R(q)$ and $E_P(q)$ can be chosen harmonic, actually with identical force constants f since the widths of the Gaussian distributions of $\Delta E(t)$ before and after transfer are very close.

An analysis of $\Delta E(t)$ resulting from MD simulations shows that eq. (7), according to eq. (2), arises through thermal excitations of low-frequency modes of the protein, the coupling being due to charge displacements associated with these modes. An important attribute of this result is that the number of modes coupled to electron transfer due to the long range of the Coulomb force is very large and, hence, large $\Delta E(t)$ values can arise through many small additive contributions without any individual mode exhibiting nonlinearities. This feature has attracted much attention and is discussed in ref. [37]. Another important result of our simulations is that the phenomenological properties assumed in stochastic descriptions like in refs. [25,35] are provided here from microscopic principles.

An example for the value of microscopic descriptions is the resulting interpretation of the solvent polarization

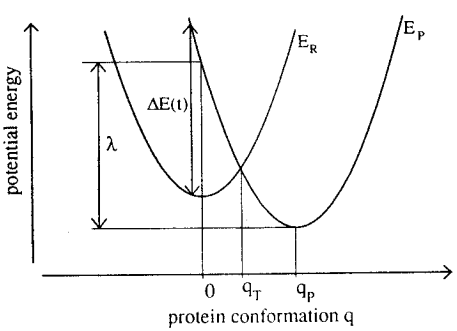

Fig. 2. Sketch of free energy curves before (E_R) and after (E_P) electron transfer as a function of a schematic one-dimensional protein conformational coordinate q. The reorganization energy λ [49] as well as the energy difference $\Delta E(t)$ for a particular $q(t)$ are indicated.

coordinate in fig. 2. In our simulations this coordinate represents the configurations of atomic partial charges in the protein. The simulations revealed that a single coordinate suffices to characterize the underlying multi-dimensional space since the quantity relevant for the medium–electron transfer coupling is actually scalar, namely the energy $\Delta E(t)$ (see eqs. (1,2)). The solvent polarization coordinate q serves merely as a parameter to represent the random occurences of $\Delta E(t)$.

A systematic study of the low-temperature limit along the line suggested by the Hamiltonian (1–3) can be carried out following the analysis of the spin–boson problem by Legget et al. [28]. This is the subject of the accompanying paper [26] which uses the present investigation to determine the suitable spin–boson Hamiltonian (1–3). The present paper establishes the properties of the medium coupling only in the classical, i.e., high-temperature, limit, however, in this limit agrees with the results reported in ref. [26].

1.7. Overview

We like to outline briefly the contents of this paper. The methods employed for our MD simulations are described in section 2. The theory which describes the coupling of electron transfer and protein motion in terms of a two-state quantum system which experiences a diagonal perturbation through the surrounding protein is presented in section 3. This section introduces as an essential mathematical tool for the study of stochastic quantum systems the line shape formalism [38,39] which provides a useful and transparent representation of the relationship between medium properties and electron transfer. It should be stressed that the approach used goes beyond the second-order perturbation methods employed in most other investigations. The results of our simulations and of the quantum mechanical description of electron transfer are presented in section 4. We conclude the paper with a summary in section 5.

2. Simulations

MD simulations were carried out using the program X-Plor/Charmm [40,41]. Our simulations are based on the X-ray structure of the photosynthetic reaction center of *Rps. viridis* [7–9]. The large size of the reaction center defies simulations over time periods as long as required for the present study. Therefore, we employed the stochastic boundary method [42,43] to confine the simulation to a subset of the reaction center. Our setup of the stochastic boundary and equilibration of the system are described in refs. [44,14]. The simulated region contained about 5800 of the 12637 reaction center atoms including all cofactors shown in fig. 1. To take into account electrostatic interactions between atoms inside the simulated sphere and charged residues in a shell from 29 to 37.5 Å, we adopted the extended stochastic boundary method as described in ref. [14]. 74 water molecules, discernable in the X-ray structure, were described by means of the TIP3 model. For Coulomb and van der Waals interactions, we employed in our simulation a cutoff radius $r_{cut} = 10$ Å. We used an integration step of 1 fs and applied the SHAKE algorithm [45] for bonds with non-water hydrogens. In order to describe the protein at various temperatures the protein was "cooled" by means of MD simulations for which the stochastic boundary layer was set at the desired temperature and, thereby, acted as a cold bath [44].

The charge distributions of neutral and ionized chromophores were taken from INDO calculations [46]. For the excited special pair P* we assumed the ground state charge distribution. All other atomic partial charges were adopted from Charmm force field parameters [41]. The charge state for the amino acids are those for pH = 7, assuming standard pK values, except for the following groups: the glutamate L104 was protonated and the Fe_I charge was changed to +2. We performed simulations at temperatures 300, 200, 120, 80, 50, and 10 K. It is certainly not appropriate to describe a protein classically at very low temperatures as remarked in section 1.

For each temperature, we distinguish three simulation phases. A first 25 ps phase denoted by "$P_S H_L Q_A$"

describes the reaction center before any electron transfer; in this phase all chromophores are neutral. A second 10 ps phase, denoted by "$P_S^+ H_L^- Q_A$", describes the protein after electron transfer $P_S \rightarrow H_L$ with P_S positively charged and H_L negatively charged. A third 5 ps phase, denoted by "$P_S^+ H_L Q_A^-$", describes the protein after electron transfer $H_L \rightarrow Q_A$ with P_S positively charged and Q_A negatively charged. In some cases, e.g. for the calculations at 300 K, the simulation times were actually longer to improve statistics. Electron transfer was modeled by instantaneously changing the charge distributions of the involved chromophores according to the INDO charge distributions mentioned above.

Dielectric fluctuation and relaxation accompanying electron transfer were monitored by calculation of the energy difference $\Delta E_{MD}(t)$ between reactant state (before electron transfer, index R) and product state (after electron transfer, index P). As discussed in section 1, $\Delta E_{MD}(t)$ governs the quantum mechanical transition between reactant and product states. Due to the motion of the protein represented by a multi-dimensional configuration vector $\boldsymbol{q}(t)$, the energy difference

$$\Delta E_{MD}(t) = E_P[\boldsymbol{q}(t)] - E_R[\boldsymbol{q}(t)] \tag{8}$$

between the two states is fluctuating in time. When the protein motion is simulated with chromophore charge distributions according to the reactant state, $\Delta E_{MD}(t)$ corresponds to the energy required to *instantaneously* transfer an electron from reactant to product state without changing the nuclear conformation. Likewise, after an electron transfer, $-\Delta E_{MD}(t)$ is the energy required for a transfer from the product state back to the reactant state.

The energy difference $\Delta E_{MD}(t)$ connected with a virtual electron transfer was determined on the basis of the MD trajectory $\boldsymbol{q}(t)$ as follows: protein configurations $\boldsymbol{q}(t)$ were sampled at 5 fs intervals; for each configuration the potential energy was evaluated twice, once with chromophore charge distributions corresponding to state R to obtain $E_R[q(t)]$, and once with chromophore charge distributions corresponding to state P to obtain $E_P[q(t)]$; we then determined $\Delta E_{MD}(t) = E_R[q(t)] - E_P[q(t)]$. For this evaluation we employed a cutoff radius of 40 Å, a choice discussed in section 4.1. We carried out the same calculations also in 1 fs intervals rather than in 5 fs intervals. The results showed that the longer time intervals yield smooth representations of $\Delta E(t)$, i.e., a representation without artificial discontinuities and artificial Fourier components.

In our MD simulations we obtain $\Delta E_{MD}(t)$ only within an additive constant encompassing redox and Born energies since $\Delta E_{MD}(t)$ contains only contributions of the protein matrix. The associated contribution of the protein matrix λ_{prot} to the reorganisation energy [47] (see fig. 2) is

$$\lambda = \tfrac{1}{2}(\langle \Delta E_{MD} \rangle_P - \langle \Delta E_{MD} \rangle_R) = -\tfrac{1}{2}\Delta\Delta E\,. \tag{9}$$

Here $\langle\ \rangle_{R,P}$ denote the time averages of ΔE_{MD} in the state of R or P. The actual reorganization energy for a protein needs to be scaled by the high-frequency dielectric constant due to electronic polarizability ϵ, i.e., $\lambda_{prot} = \lambda/\epsilon$. Likewise, one finds that the free energy difference between the reactant state and the product state, i.e., the quantity ϵ_0 in eq. (6), can be expressed as

$$\epsilon_0 = \tfrac{1}{2}(\langle \Delta E_{MD} \rangle_P + \langle \Delta E_{MD} \rangle_R)\,. \tag{10}$$

3. Electron transfer theory

In this section we describe the effect of thermal fluctuations of $\Delta E_{MD}(t)$ on electron transfer rates. For this purpose we adapt existing electron transfer theories in solution [33,34,47,48,25,35]. MD simulations treat the protein motion classically, i.e., such simulations do not properly account for intramolecular high-frequency motions which require a quantum mechanical description. Hence, our simulations can only describe coupling of the transfer process to classical motions of the protein matrix. To motivate our expression for the electron transfer rate we consider here Fermi's golden rule, replacing this approximation later. We assume, following

Sumi and Marcus [25], that two classes of motion couple to electron transfer, high-frequency vibrations with a final state energy density $\mathscr{S}_{qm}(E)$ and classical degrees of freedom with a final state energy density $\mathscr{S}_{cl}(E)$. Fermi's golden rule approximates then the transfer rate as follows

$$\tilde{k}_{R\to P}=\frac{2\pi}{\hbar}|V|^2\int_{-\infty}^{+\infty}\mathrm{d}\epsilon\,\mathscr{S}_{cl}(\epsilon)\,\mathscr{S}_{qm}(-\epsilon)\,. \tag{11}$$

Here $\mathscr{S}_{qm}(E)$ can also account for the electronic and Born energy contributions to the redox energy $E_{\text{redox-Born}}$ by shifting its energy scale accordingly (see section 4.5). The functions $\mathscr{S}_{qm}(E)$ and $\mathscr{S}_{cl}(E)$ depend only on the static level density and Boltzmann distribution in the initial states and expression (11) can only hold as long as the relaxation times governing the motion of the nuclear degrees of freedom are long compared to the time scale relevant for the electron transfer process. If one assumes that this condition for the relaxation times does not hold for the classical degrees of freedom, one needs to describe the electron transfer rate in a manner which accounts explicitly for the time-dependence of the coupling between the classical degrees of freedom and electron transfer. Let us assume that the latter description results in a rate $k_{cl}(\epsilon)$. To obtain the rate which includes the effect of both the classical and the quantum mechanical degrees of freedom, one needs to replace eq. (11) by

$$k_{R\to P}=\int_{-\infty}^{\infty}\mathrm{d}\epsilon\,k_{cl}(\epsilon)\,\mathscr{S}_{qm}(-\epsilon)\,. \tag{12}$$

This description corresponds to the use of a "reaction window" in ref. [35], the width of which is described by $\mathscr{S}_{qm}(E)$.

We outline here only briefly the properties of the line shape function $\mathscr{S}_{qm}(E)$ assuming that a small number of quantum mechanical degrees of freedom are included in the description, and that these degrees of freedom are harmonic. In this case $\mathscr{S}_{qm}(E)$ is the Franck–Condon and Boltzmann-weighted energy density of final states given by the convolution

$$\mathscr{S}_{qm}(E)=\int\mathrm{d}E_1\int\mathrm{d}E_{2\ldots}\int\mathrm{d}E_N\left[\prod_{j=1}^{N}S_j(E_j)\right]\delta\left(\sum_{j=1}^{N}E_j-E-E_{\text{redox-Born}}\right). \tag{13}$$

Each of the line shape functions $S_j(E)$ describes a single harmonic degree of freedom and is [50]

$$S_j(E)=\frac{\mathrm{e}^{-\lambda_j(1+2n_j)}}{\hbar\omega_j}\left(\frac{n_j+1}{n_j}\right)^{s_j/2}\sum_{k=-\infty}^{\infty}\delta(k-s_j)I_{s_j}\left(2\lambda_j\sqrt{n_j(n_j+1)}\right), \tag{14}$$

where $\lambda_j=\frac{1}{2}fq_j^2/\hbar\omega_j$ is the reorganization energy of that degree of freedom in units of vibrational quanta, $n_j=\mathrm{e}^{-\hbar\omega/kT}/(1-\mathrm{e}^{-\hbar\omega_j/kT})$ is the average number of quanta thermally excited in the oscillator, $s_j=(E-E_{0j})/(\hbar\omega_j)$ counts the oscillator levels, and I_m denotes the regular, modified Bessel function of integer order [51]. Expressions (13,14), originally developed to describe optical transitions in solids [50], were introduced to thermal electron transfer by Jortner [52,49].

We focus our attention in this paper only on the properties of the classical contribution to the transfer rate k_{cl}. In fact, in our simulations below all degrees of freedom, including intramolecular vibrations of the chromophores, were described classically. This implies the functional form $\mathscr{S}_{qm}(-\epsilon)=\delta(\epsilon-E_{\text{redox}}-E_{\text{Born}})$ and implies that the ϵ-dependence of $k_{cl}(\epsilon)$ can be interpreted as a dependence of the transfer rates on redox energy. A quantum mechanical description has been completed by us recently [26].

3.1. Two-state model coupled to classical medium

We consider electron transfer as a transition in a two-level quantum system, one level representing the state R before electron transfer, the other level representing the state P after electron transfer. The two states are separated by the energy $\Delta E_{\mathrm{MD}}(t)$ which fluctuates in time. Electron transfer is described by a two-state density matrix $\rho(t)$ which obeys the Liouville equation

$$\partial_t \rho(t) = \frac{\mathrm{i}}{\hbar}[\mathscr{H}(t), \rho(t)]_- - [\mathscr{K}, \rho(t)]_+, \quad \mathscr{H}(t) = \begin{pmatrix} \epsilon & V \\ V & \Delta E_{\mathrm{MD}}(t) \end{pmatrix}, \quad \mathscr{K} = \begin{pmatrix} 0 & 0 \\ 0 & \tau^{-1} \end{pmatrix}. \tag{15}$$

Here $\mathscr{H}(t)$ is the Hamiltonian of the two-state system. The parameter ϵ represents the energy "exchanged" with the degrees of freedom described by $\mathscr{S}_{\mathrm{qm}}(\epsilon)$ (see eq. (12)), $\Delta E_{\mathrm{MD}}(t)$ introduces the fluctuating energy difference between reactant and product states, and V couples both states. The operator $\mathscr{K}$ describes relaxation of the system in state P. We employed the notation $[A, B]_\pm = AB \pm BA$. ρ_{11} is the probability to find the system in the reactant state. The initial condition is $\rho_{11}=1$, $\rho_{12}=\rho_{21}=\rho_{22}=0$. Shifting both of its diagonal elements by $\frac{1}{2}(\Delta E_{\mathrm{MD}}(t)-\epsilon)$ converts $\mathscr{H}(t)$ into the operator $\mathscr{H}'$ introduced in eq. (3). It should be noted that the solution of eq. (15) is exact to all orders in V, rather than only to second order as in the common descriptions involving Fermi's golden rule.

In contrast to a classical picture [33,34,47] in which, due to weak coupling between reactant and product states, an electron can only be transfered when the energies of the two states are approximately equal – in terms of fig. 2 at the point $\boldsymbol{q} \approx \boldsymbol{q}_T$ – the two-state model, in principle, permits transfer for all protein conformations.

The solution of eq. (15) for a *piecewise time-independent* Hamiltonian $\mathscr{H}$ is

$$\rho(t+\Delta t) = \mathscr{P}\rho(t)\mathscr{P}^\dagger, \quad \mathscr{P} = \exp\left[\Delta t\left(\frac{\mathrm{i}}{\hbar}\mathscr{H} - \mathscr{K}\right)\right]. \tag{16}$$

Evaluating the exponential operator through Taylor expansion and grouping terms of odd and even powers yields

$$\rho(t+\Delta t) = \left(\cos \Delta t\gamma \mathbb{1} + \mathrm{i}\frac{\sin \Delta t\gamma}{\gamma}\mathbf{A}\right)\rho(t)\left(\cos \Delta t\bar{\gamma}\mathbb{1} - \mathrm{i}\frac{\sin \Delta t\bar{\gamma}}{\bar{\gamma}}\bar{\mathbf{A}}\right)\mathrm{e}^{-t/\tau}, \tag{17}$$

where $\mathbb{1}$ stands for the identity matrix, $\bar{\gamma}$, $\bar{\mathbf{A}}$ denote the complex conjugate of γ, $\mathbf{A}$, and the abbreviations

$$\gamma = \sqrt{\Omega^2 + \omega^2}, \quad \omega = V/\hbar, \quad \Omega = \frac{1}{2\hbar}\left(\Delta E_{\mathrm{MD}} - \epsilon - \frac{\mathrm{i}\hbar}{\tau}\right), \quad \mathbf{A} = \begin{pmatrix} \Omega & \omega \\ \omega & -\Omega \end{pmatrix} \tag{18}$$

are used. Within a mono-exponential approximation for the decay of $\rho_{11}(\epsilon, t)$ holds

$$[k_{\mathrm{cl}}^{\mathrm{MD}}(\epsilon)]^{-1} = \int_0^\infty \mathrm{d}t\, \rho_{11}(\epsilon, t), \tag{19}$$

where we have denoted an ϵ-dependence of ρ and of $k_{\mathrm{cl}}^{\mathrm{MD}}$ which arises through eq. (18). In section 4.5 we will present the transfer rates $k_{\mathrm{cl}}^{\mathrm{MD}}(\epsilon)$ obtained by this approach. We note finally that the scale for ϵ chosen here is such that the rate assumes its maximum at $\epsilon_{\max} = \langle \Delta E_{\mathrm{MD}} \rangle_{\mathrm{R}}$.

3.2. Two-state model coupled to stochastic medium

The key property of the protein matrix which enters into the two-state model of electron transfer is the energy difference $\Delta E_{\mathrm{MD}}(t)$. The question arises in how far a cumbersome simulation of the whole protein is necessary

to provide this quantity. Does a stochastic model exist that can provide $\Delta E_{ST}(t)$, which, when entered into the two-state Hamiltonian (15) instead of $\Delta E_{MD}(t)$, reproduces the transfer rates k_{el}^{MD}? Such stochastic process may also allow one to investigate which characteristics of $\Delta E_{MD}(t)$ are essential in determining the transfer rate, i.e., which characteristics need to be controlled by a protein to optimize electron transfer. In the following we will introduce the most rudimentary stochastic process possible which is chosen to reproduce three statistical properties of $\Delta E_{MD}(t)$, namely the mean value $\langle \Delta E_{MD} \rangle$, the rms-deviations σ from the mean, and the mean relaxation time τ of fluctuations of $\Delta E_{MD}(t)$. We will find further below that the corresponding model qualitatively reproduces the rate $k_{el}^{MD}(\epsilon)$, but with a narrower ϵ-dependence.

The stochastic process we suggest is the so-called Ornstein–Uhlenbeck process described by the Fokker–Planck equation [53,54]

$$\partial_t p(u,t) = \mathcal{L} p(u,t), \quad \mathcal{L} = D \partial_u p_0(u) \partial_u [p_0(u)]^{-1} . \tag{20}$$

Here $p(u,t)$ is the probability to observe for the stochastic variable a value u at time t. The probability distribution $p(u,t)$ as described by eq. (20) converges asymptotically towards the (equilibrium) distribution $p_0(u)$, i.e., $\lim_{t\to\infty} p(u,t) = p_0(u)$ which, for an Ornstein–Uhlenbeck process, is a Gaussian with width σ and mean $\langle u \rangle$

$$p_0(u) = \frac{1}{\sqrt{2\pi\sigma}} \exp[-(u-\langle u \rangle)^2/2\sigma^2] . \tag{21}$$

The parameter D in eq. (20) governs the temporal behavior of the Ornstein–Uhlenbeck process. One can derive [54] that the equilibrium correlation function

$$C(t) = \frac{\langle u(t)u(0) \rangle - \langle u \rangle^2}{\langle u^2 \rangle - \langle u \rangle^2} \tag{22}$$

exhibits a simple exponential decay governed by D

$$C(t) = \exp[-2Dt/\sigma^2] . \tag{23}$$

The Ornstein–Uhlenbeck process can be employed to model an "observed" random process $\xi(t)$. This is possible if the distribution function $\tilde{p}_0(\xi)$ obtained from a long time sampling of $\xi(t)$, i.e., of $\Delta E_{MD}(t)$, is Gaussian. Comparison of $\tilde{p}_0(\xi)$ with eq. (21) yields the parameters $\langle u \rangle$ and σ. Furthermore, the correlation function of the process expressed through the time average

$$\tilde{C}(t) = \lim_{t_0\to\infty} \frac{1}{t_0} \int_0^{t_0} dt' \, \frac{\xi(t+t')\xi(t') - \langle \xi \rangle^2}{\langle \xi^2 \rangle - \langle \xi \rangle^2} \tag{24}$$

must be approximated well through a mono-exponential

$$\tilde{C}(t) \approx \exp[-t/\tau] . \tag{25}$$

This approximation allows one to identify D through $D = \sigma^2/2\tau$ (cf. eqs. (23,25)). In our simulations we have determined $\tilde{C}(t)$ actually through

$$\tilde{C}(t) = \frac{1}{M} \sum_{j=1}^{M} \frac{\xi(t+t_j)\xi(t_j) - \langle \xi \rangle^2}{\langle \xi^2 \rangle - \langle \xi \rangle^2} \tag{26}$$

for $M = 20$ and where t_j denotes time instances along the trajectory which were spaced by 1 ps; the time course of $\tilde{C}(t)$ for each t_j was monitored over a time span of 5 ps.

We want to describe now $\Delta E_{MD}(t)$ through an Ornstein–Uhlenbeck process. One can establish the parameters which determine such a process by monitoring in an MD simulation the following: the equilibrium distribution $\tilde{p}_0(\Delta E_{MD})$ and the equilibrium autocorrelation function $\tilde{C}(t)$ defined according to eq. (26) with $\xi(t) = \Delta E_{MD}(t)$.

One can then readily determine $\langle u\rangle$, σ, and D. We will see below that $\tilde{p}_0(\Delta E)$ is, in fact, very close to a Gaussian and that the correlation function can be approximated by a mono-exponential; however, the latter approximation is not completely satisfactory.

By employing the theory in refs. [39,36] one can express the density matrix

$$\rho(\epsilon|t)=\int \mathrm{d}\Delta E'\, \mathscr{I}(\Delta E')\rho_0(\epsilon-\Delta E'|t)\,, \tag{27}$$

where

$$\rho_0(\epsilon-\Delta E'|t)=\exp\left[-\frac{\mathrm{i}t}{\hbar}\begin{pmatrix}\epsilon & V\\ V & \Delta E'-\mathrm{i}\hbar/\tau\end{pmatrix}\right]\begin{pmatrix}1 & 0\\ 0 & 0\end{pmatrix}\exp\left[\frac{\mathrm{i}t}{\hbar}\begin{pmatrix}\epsilon & V\\ V & \Delta E'+\mathrm{i}\hbar/\tau\end{pmatrix}\right]. \tag{28}$$

Here $\rho_0(\epsilon-\Delta E'|t)$ expresses the density matrix for a Hamiltonian (15) with a *time-independent* energy term $\Delta E'$, i.e., it can be evaluated by means of eqs. (17,18). $\mathscr{I}(\Delta E')$ represents the Kubo line shape function [38]

$$\mathscr{I}(\Delta E')=\frac{1}{\pi}\mathrm{Re}\left\langle 0\left|\frac{1}{(\mathrm{i}/\hbar)(u-\Delta E')-\mathscr{L}}\right|0\right\rangle. \tag{29}$$

Expressions (27–29) yield an approximation accurate to third order in V which, however, accounts also for contributions of all orders of V [39]. This approximation conserves the trace of the density matrix and converges to the exact results in the limits of both slow or fast stochastic motion measured on a scale $\hbar/V$ [38]. A numerical method for the evaluation of the line shape function (29) is described in appendix A. We will demonstrate below that, in the present case, the approximation corresponding to eqs. (27–29) is accurate. We like to emphasize that the description given goes beyond second-order perturbation theory in that all orders of V contribute.

In order to determine the rate $k_{\mathrm{el}}^{\mathrm{ST}}(\epsilon)$ we proceed in a way which differs from that suggested in ref. [36] yielding a numerically more stable approximation. We note that eq. (18) implies that the density matrix element $[\rho(\epsilon|t)]_{11}$ is approximated by a single exponential

$$[\rho(\epsilon|t)]_{11}\approx\exp[-k_{\mathrm{el}}^{\mathrm{ST}}(\epsilon)t)]\,. \tag{30}$$

We assume the same approximation for the (1, 1) element of $\rho_0(\epsilon-\Delta E'|t)$, i.e.,

$$[\rho_0(\epsilon-\Delta E'|t)]_{11}\approx\exp[-k_0(\epsilon-\Delta E')t] \tag{31}$$

and establish $k_0(\epsilon-\Delta E')$ through the identity

$$[k_0(\epsilon-\Delta E')]^{-1}=\int_0^\infty \mathrm{d}t\,[\rho_0(\epsilon-\Delta E'|t)]_{11} \tag{32}$$

which holds if eq. (31) holds exactly. (Note that we do not define the rates through the time derivative of the density matrix element itself since, of course, this derivative vanishes at $t=0$.) One can conclude then from eq. (27)

$$\exp[-k_{\mathrm{el}}^{\mathrm{ST}}(\epsilon)t]\approx\int \mathrm{d}\Delta E'\, \mathscr{I}(\Delta E')\exp[-k_0(\epsilon-\Delta E')t]\,. \tag{33}$$

Differentiating both sides at $t=0$ yields

$$k_{\mathrm{el}}^{\mathrm{ST}}(\epsilon)\approx\int \mathrm{d}\Delta E'\, \mathscr{I}(\Delta E')\, k_0(\epsilon-\Delta E')\,. \tag{34}$$

In the present case three parameters determine the functional form of $\mathscr{I}(\Delta E)$. A first parameter is $\langle u\rangle=\langle\Delta E\rangle$ and, according to eq. (21), determines the center of $\mathscr{I}(\Delta E)$ on the ΔE axis. A second parameter is σ [see eq.

(21)]. This parameter can be absorbed into the scale of the ΔE-axis. The corresponding line shape function is then, using $u' = u/\sigma$, $\Delta\epsilon = \Delta E/\sigma$,

$$\mathcal{J}(\Delta\epsilon) \sim \mathrm{Re}\left\langle 0 \left| \frac{1}{\mathrm{i}(u' - \Delta\epsilon) - \rho \partial_{u'} p_0(u') \partial_{u'} [p_0(u')]^{-1}} \right| 0 \right\rangle , \tag{35}$$

which expresses the line shape function in dimensionless variables. Here,

$$\rho = D\hbar/\sigma^3 \tag{36}$$

is the single dimensionless parameter which describes the dynamic effect of fluctuations $\Delta E(t)$, large ρ values corresponding to rapid fluctuations. Since the effect of $\langle u \rangle$ and σ can be absorbed through shift and scaling of the ΔE-axis, the parameter ρ constitutes the essential parameter which determines the shape of $\mathcal{J}(\Delta E)$.

3.3. Relationship to Marcus theory

The description in terms of eqs. (34,29) makes the dependence of the electron transfer rate on the stochastic properties of the medium, i.e., on $\langle \Delta E \rangle$, σ and ρ, transparent. This dependence is accounted for by the line shape function (29, 35). In the limit $\rho \to 0$ this function converges to the distribution $\tilde{p}_0(\Delta E)$ [38]. In this limit the rate $k_{\mathrm{cl}}^{\mathrm{ST}}(\epsilon)$ is then essentially the same as the rate described by the Marcus theory [33,34]. This can be seen as follows.

The rate $k_0(\epsilon - \Delta E)$, defined in eq. (31), assumes significant values only in a narrow range of width V around $\epsilon \approx \Delta E$. One may, in fact, assume that the rates $k_0(\epsilon - \Delta E)$ vanish, except at $\epsilon = \Delta E' = 0$, where the rates can be determined according to

$$[\hat{k}_0]^{-1} = \tau \int_0^\infty \mathrm{d}t\, \mathrm{e}^{-t} \left(\cos t\gamma' + \frac{\sin t\gamma'}{2\gamma'\tau} \right)^2 ; \quad \gamma' = \frac{1}{2} \sqrt{\left(\frac{4V\tau}{\hbar} \right)^2 - 1} ; \quad \frac{4|V|\tau}{\hbar} > 1 . \tag{37}$$

One can then state $k_{\mathrm{cl}}^{\mathrm{ST}}(\epsilon) \sim \hat{k}_0 \hat{p}_0(\epsilon)$. In second-order perturbation theory would hold

$$k_0 = \frac{2\pi V^2}{\hbar} \delta(\Delta E - \epsilon) \tag{38}$$

and, hence,

$$k_{\mathrm{cl}}^{\mathrm{ST}}(\epsilon) = \frac{2\pi V^2}{\hbar} \tilde{p}(\epsilon) . \tag{39}$$

We like to show now that the factor $\tilde{p}_0(\epsilon)$ reproduces the ΔG_0-dependence of the Marcus theory. We first note that $\tilde{p}_0(\Delta E)$ describes the probability that reactant and product states are separated by the energy ΔE. In case of potentials $E_{\mathrm{R}}(q)$ and $E_{\mathrm{P}}(q)$ defined in eq. (6) and for an initial Boltzmann distribution in $E_{\mathrm{R}}(q)$ one can derive (see for example ref. [36])

$$\tilde{p}_0(\Delta E) = \frac{1}{\sqrt{2\pi f k T q_{\mathrm{P}}}} \exp\left[- \frac{(\Delta E + \epsilon_0 - \frac{1}{2} f q_{\mathrm{P}}^2)^2}{2kTfq_{\mathrm{P}}^2} \right] . \tag{40}$$

We note further that, according to the Marcus theory, the corresponding electron transfer rate $k_{\mathrm{cl}}^{\mathrm{Ma}}(\epsilon_0)$ is proportional to the Arrhenius factor determined by the point q_T of intersection of $E_{\mathrm{R}}(q)$ and $E_{\mathrm{P}}(q)$ depicted in fig. 2

$$k_{\mathrm{cl}}^{\mathrm{Ma}}(\epsilon_0) \approx \sqrt{\frac{f}{2\pi kT}} \exp\left[- \frac{E_{\mathrm{R}}[q_T(\epsilon_0)]}{kT} \right] . \tag{41}$$

One readily derives $q_T(\epsilon_0) = (\frac{1}{2}fq_P^2 - \epsilon_0)/fq_P$ and, hence,

$$k_{cl}^{Ma}(\epsilon_0) \approx \frac{1}{\sqrt{2\pi fkTq_P}} \exp\left[-\frac{(\epsilon_0 - \frac{1}{2}fq_P^2)^2}{2kTfq_P^2}\right], \tag{42}$$

where we have renormalized eq. (41) to energy space. Obviously, eqs. (40) and (42) represent the same dependence on ϵ_0, i.e., on ΔG_0. We conclude, therefore, that in the limit $\rho \to 0$ the stochastic quantum mechanical model and the Marcus theory yield the same dependence of the transfer rate on ΔG_0.

In the so-called motional narrowing limit of very large ρ the line shape function $\mathscr{I}(\Delta E)$ coalesces to the δ-function $\delta(\Delta E - \langle \Delta E \rangle)$. However, this limit is hypothetical since ρ is about 0.03 for the simulations presented below. One may expect, however, that any $\rho > 0$ leads to an ϵ_0-dependence of the transfer rates k_{cl}^{ST} which is narrower than that predicted by the Marcus theory.

3.4. Relationship to $\mathscr{S}_{qm}(\epsilon)$

A broadening of $k_{cl}^{ST}(\epsilon_0)$ can arise due to medium vibrational modes with frequencies of the order of $\sigma/\hbar$. For an explanation we consider a two-state system as studied by Kubo [38]. If the states are described by the Hamiltonian $\mathscr{H}(t)$ defined in eq. (15) then, even in case $|V| < \epsilon$ and ϵ significantly larger than $|\Delta E(t)|$, a transition between the states can be induced in case $\Delta E(t)$ has suitable Fourier components. The motion giving rise to $\Delta E(t)$ can "lend" or "borrow" energy needed for the transition. This contribution, to a large degree, is equivalent to a description incorporating in eq. (12) quantum mechanical vibrational modes through the factor $\mathscr{S}_{qm}(\epsilon)$ providing, thereby, a "broad reaction window" [35]. The reason why a classical oscillator can resemble a quantum mechanical oscillator in that it exchanges with another quantum systems energy quanta $\hbar\omega$ arises from the fact that a classical oscillator, irrespective of its amplitude, has the same frequency ω. A distinction between a classical and a quantum oscillator is, however, that the latter has a nonvanishing amplitude and, hence, nonvanishing interaction even at very low temperature.

To prove the limitation to energy exchange $\pm\hbar\omega$ between classical oscillator and quantum electron transfer system we consider Hamiltonian (1) in a form which assumes that the coupling $\delta E(t)$ describes the contribution of a single oscillator of frequency ω

$$\mathscr{H}'(t) = \sigma_1 V + (\delta_0 + \delta_1 \cos\omega t)\sigma_3 . \tag{43}$$

As is well-known [55], the time evolution of the density matrix of such systems, described by the three-dimensional vector $\boldsymbol{m} = (\mathrm{Re}\,\rho_{12}, \mathrm{Im}\,\rho_{12}, \rho_{11} - \rho_{22})$, can be evaluated by means of the Bloch equation

$$\frac{\mathrm{d}}{\mathrm{d}t}\boldsymbol{m} = \frac{1}{\hbar}\boldsymbol{m} \times \boldsymbol{H}(t); \quad \boldsymbol{H} = (V, 0, \delta_0 + \delta_1 \cos\omega t) . \tag{44}$$

One can transform the three-dimensional coordinate system in which $\boldsymbol{m}$ and the "field" $\boldsymbol{H}$ are defined such that the new z-axis points along the time-independent vector $\boldsymbol{H}_0 = (V, 0, \delta_0)$. For $\delta_0 \gg |V|$, the case considered here, this transformation does not affect in an essential way the interpretation of m_3 as the difference between reactant and product state occupancy. In the transformed system acts the time-dependent "field" ($\delta_0 \gg |V|$, $\delta_0 \gg \delta_1$)

$$\boldsymbol{H} = (\delta_1 V/\delta_0, 0, \delta_1) \cos\omega t . \tag{45}$$

For $\hbar\omega \approx \delta_0$ the effect of this field can be accounted for by transforming to a frame rotating with frequency $\pm\omega$ around the new z-axis and assuming in the rotating frame the effective static field

$$\boldsymbol{H}_{\mathrm{eff}} = (\delta_1 V/\delta_0, 0, \delta_0 \mp \hbar\omega) . \tag{46}$$

This field induces transitions between reactant and product states on a time scale $\tau = \delta_0\hbar/|V|\delta_1$. In the present case of electron–vibrational coupling this time scale is a critical parameter determining the relevance of the

interaction considered. Assuming $\delta_0/|V| \approx 10^3$ and a coupling strength δ_1 of 0.2 kcal/mol for a single vibrational mode one estimates $\tau \approx 10$ ps. One must note that, because of the resonance condition $\hbar\omega \approx \delta_0$, only protein vibrations in the frequency range $(\delta_0 \pm V)/\hbar$ contribute to the effect described.

It is also important to realize that the description given here does not conserve energy of the combined electron–nuclear system, a feature which may not matter at high temperatures, but certainly does at low temperatures. As discussed below, the fact that the transfer rates $k_{cl}^{MD}(\epsilon)$ originating from $\Delta E_{MD}(t)$ have a very broad ϵ-dependence attests to the relevance of the coupling between electron transfer and vibrational modes described here.

4. Results

First, we present some results which hold for the electron transfer $P_S \rightarrow H_L$ as well as $H_L \rightarrow Q_A$.

4.1. $\Delta E_{MD}(t)$ and the range of Coulomb interaction

We investigated the dependence of $\Delta E_{MD}(t)$ on the cut-off radius r_{cut} used for calculating $\Delta E_{MD}(t)$ and observed that the absolute values of $\Delta E_{MD}(t)$ depend sensitively on r_{cut}. This dependence is presented in fig. 3. One can recognize that changes in r_{cut} alter dramatically the values of $\Delta E_{MD}(t)$. There are two aspects to this. First, our findings require one to include in a calculation of $\Delta E_{MD}(t)$ a very large number of atomic partial charges, i.e., even those far away from a donor–acceptor pair. Second, the result in fig. 3 demonstrates that the influence of the protein on electron transfer does not stem from a small number of groups, e.g., some groups close to a donor–acceptor pair, but rather involves collective motion involving essentially the whole protein, possibly also the protein environment, i.e., a membrane fraction and water. This feature implies that charge neutralization in the protein does not lead to nearly complete cancellation of the coupling of the medium to the electron transfer, but rather that a significant coupling remains and increases with increasing volume. A further result is presented in fig. 4 which compares two sets of $\Delta E_{MD}(t)$ values evaluated for different r_{cut} values. The results show that even though the absolute values of $\Delta E_{MD}(t)$ are rather dependent on r_{cut}, the fluctuations for different r_{cut} are qualitatively similar, except that the magnitude of fluctuations of $\Delta E_{MD}(t)$ significantly in-

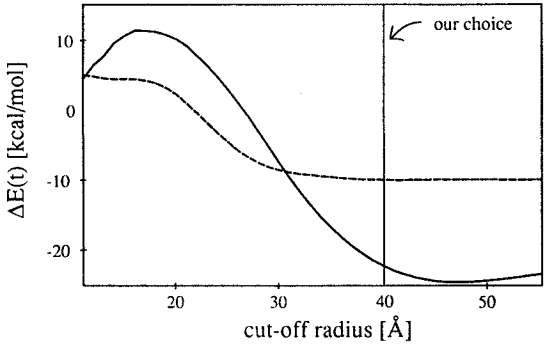

Fig. 3. ΔE_{MD} values as a function of the cutoff radius r_{cut} evaluated for the reactant phases of the electron transfers $P_S \rightarrow H_L$ (solid line) and $H_L \rightarrow Q_A$ (dashed line). To determine ΔE_{MD} we halted the simulations in phase $P_S H_L Q_A$ and in phase $P_S^+ H_L^- Q_A$ at one time instance $t^\dagger$ and evaluated $\Delta E_{MD}(t^\dagger)$ for various values of r_{cut}.

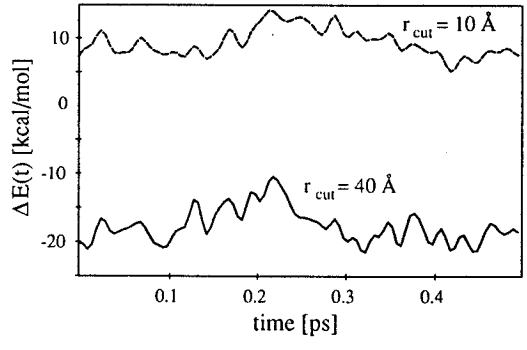

Fig. 4. $\Delta E_{MD}(t)$ for two values of the cutoff radius r_{cut}, analyzed for the electron transfer $P_S \rightarrow H_L$ before transfer.

creases with increasing cutoff radii. The $\Delta E_{MD}(t)$ values below all have been evaluated with an r_{cut} value of 40 Å.

Fig. 4 demonstrates also the important fact that the fluctuations of $\Delta E_{MD}(t)$ exceed the electronic coupling V by three orders of magnitude, i.e., one can certainly expect a significant coupling between protein motion and electron transfer.

4.2. Distances and mobilities of cofactors

The electron transfer rate through the electronic matrix element depends on the donor–acceptor distance. To determine center–center distances, we first determined a geometrical center of each chromophore by averaging over the central ring atoms (atoms involved in bonds drawn as thick lines in fig. 1). Our simulations yield the following main results. Together with an overall contraction of the reaction center upon cooling [44], all average distances as well as fluctuations of the distances between chromophores decrease with lowering the temperature. As a result of the charge transfers, the distances are not changed significantly, except in the case of the Q_A–Q_B distance as discussed in section 4.4. Typical center–center distances are presented for two temperatures in fig. 5.

The chromophore mobilities, measured by averaging rms-deviations of the central ring atoms (see fig. 1) of each chromophore, decrease almost linearly when the temperature is lowered. Typical values for a bacteriochlorophyl or a bacteriopheophytin are 0.25 Å at 300 K and 0.05 Å at 50 K. The mobilities of corresponding chromophores for the two branches are very similar; for certain temperatures the mobilities in the L-branch are higher than those in the M-branch, for others the mobilities in the L-branch are smaller than those in the M-branch.

4.3. Electron transfer $P_S \rightarrow H_L$

Comparison of simulated, averaged structures before and after the electron transfer $P_S \rightarrow H_L$ reveals no major structural changes induced by the transfer, i.e., the respective differences in atomic positions and the differences of center–center distances of cofactors are significantly smaller than the fluctuations due to thermal motions.

In fig. 6, the energy difference $\Delta E_{MD}(t)$ between the reactant state $P_S H_L Q_A$ and the product state $P_S^+ H_L^- Q_A$ is shown for different temperatures before and after the electron transfer. In fig. 7, the distributions $\tilde{p}_0(\Delta E)$ before and after electron transfer $P_S \rightarrow H_L$ are depicted for different temperatures. It is noteworthy that the distributions $\tilde{p}_0(\Delta E)$ are well matched by Gaussians, an issue discussed in ref. [36].

The features of $\Delta E_{MD}(t)$ immediately recognized in figs. 6, 7 are the following. Before the transfer, $\Delta E_{MD}(t)$ fluctuates around a mean value $\langle \Delta E_{MD} \rangle_R$. This mean value $\langle \Delta E_{MD} \rangle_R$ decreases with decreasing temperature. Within about 100 fs after the transfer $\Delta E_{MD}(t)$ relaxes towards a lower mean value $\langle \Delta E \rangle_P$. This rapid dielectric relaxation was found at all temperatures. After relaxation $\Delta E_{MD}(t)$ fluctuates around a new mean value $\langle \Delta E_{MD} \rangle_P$.

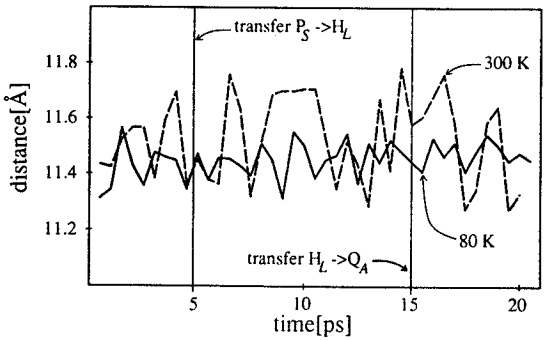

Fig. 5. Center–center distances between P_S and B_L at 300 and 80 K. Each distance was averaged over a time interval of 0.5 ps. At $t=5$ ps an electron was transfered from P_S to H_L and at $t=15$ ps from H_L to Q_A.

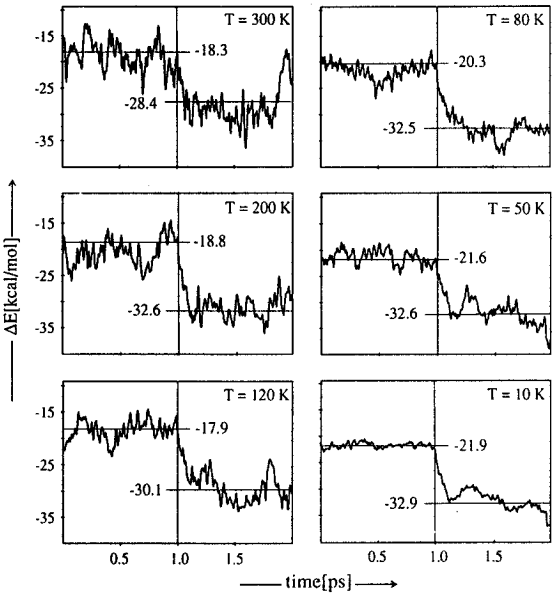

Fig. 6. $\Delta E_{MD}(t)$ for the electron transfer $P_S \rightarrow H_L$ at different temperatures. Only the last picosecond before and the first picosecond after the electron transfer are displayed. At $t = 1.0$ ps, an electron was transfered by altering the charge distributions of the cofactors P_S and H_L. The mean values of $\Delta E_{MD}(t)$ were averaged over a 10 ps time span before and over 5 ps after the transfer.

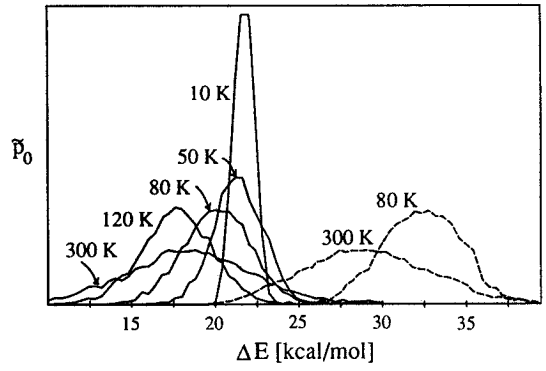

Fig. 7. Distributions $\tilde{p}_0(\Delta E_{MD})$ before (solid) and after (dashed) electron transfer $P_S \rightarrow H_L$ at different temperatures. For evaluation of the distributions after the transfer the first picosecond was omitted. The energy axis presents actually negative values.

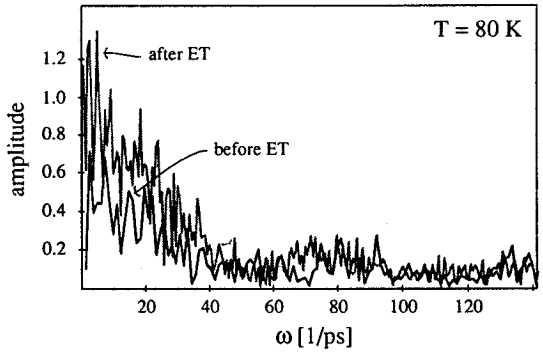

Fig. 8. Fourier spectrum of $\Delta E_{MD}(t)$ before and after the electron transfer $P_S \rightarrow H_L$, at $T = 80$ K.

Fluctuations of $\Delta E_{MD}(t)$ decrease with decreasing temperature. The energy difference $\Delta\Delta E = \langle \Delta E_{MD} \rangle_R - \langle \Delta E_{MD} \rangle_P$ measures about 10 to 14 kcal/mol and is approximately the same at all temperatures. Assuming $\epsilon = 2$, eq. (9) yields temperature-dependent reorganisation energies λ_{prot} between 2.5 (300 K) and 3.5 kcal/mol (10 K). The free energy contribution of the protein to ΔG_0 according to eq. (10) is for the same ϵ-value in the range 11.7 (300 K) to 13.6 kcal/mol (10 K).

The fact that we find a fast and sizable dielectric response to electron transfer even at low temperatures, and that no major structural changes are induced by the transfer, together with a detailed analysis of the contributions to the "solvation" energy $\Delta\Delta E$ show the following. One cannot assign specific groups as major contributors to $\Delta\Delta E$, but rather $\Delta\Delta E$ is a sum of many small contributions. These contributions seem to be due to small reorientations of polar groups. This result has also been reported and analyzed in detail in ref. [14].

We have also determined the Fourier (cosine) spectra of $\Delta E_{MD}(t)$. All spectra in this paper were evaluated for a 5.12 ps time interval with a time resolution of 5 fs using the IMSL FFTRC [56] routine. The spectra before and after electron transfer are shown in fig. 8 at 80 K. Spectra at other temperatures are very similar. The spectra in fig. 8 show a broad band of frequencies in the range 0–40 ps^{-1}. The amplitudes on the average decrease from lower frequencies to higher frequencies. The frequency spectrum is broad, lacking distinct features; i.e., there are no dominant frequencies present. Upon lowering the temperature (by a factor of two from 300 to 80 K) the amplitudes decrease in accordance with the fluctuations shown in fig. 7. The overall frequency distribution remains unchanged, none of the frequencies get frozen out preferentially. Electron transfer leads to an overall increase of the frequency amplitudes which reflects the non-equilibrium situation of the system after a transfer.

It is of interest to compare the spectra of the energy autocorrelation function $C(t)$, essentially $\Delta\hat{E}(\omega)$, with the Fourier spectra $\hat{C}_v(\omega)$ of the velocity autocorrelation functions studied in ref. [27]. The distinction between the spectra is apparent: first, $\Delta\hat{E}(\omega)$ lacks distinct high-frequency bands. This difference may, however, be due to the fact that $C(t)$ involves contributions of many atoms whereas the velocity autocorrelation functions in ref. [27] describe single atom vibrations (see also discussion below). A second difference is that the low-frequency part of $\Delta\hat{E}(\omega)$ exhibits a band confined to frequencies below $\omega \approx 40$ ps^{-1}, whereas $\hat{C}_v(\omega)$ has a significantly broader low-frequency band. This feature indicates that the protein motions underlying the low-frequency contributions to $\Delta E_{MD}(t)$ experience less friction than in the case of single atom motion. The low frequency is also indicative of a possible role of long-wavelength, i.e., collective motions of the protein matrix. However, we have not been able to identify such contributions. Similar conclusions can be drawn regarding the spectra $\Delta\hat{E}(\omega)$ for the transfer $H_L \rightarrow Q_A$.

4.4. Electron transfer $H_L \rightarrow Q_A$

The transfer $H_L \rightarrow Q_A$ was studied at temperatures 80 and 300 K. In contrast to the electron transfer $P_S \rightarrow H_L$, which is not accompanied by any significant structural rearrangement, we find a significant structural response in case of $H_L \rightarrow Q_A$. This response is depicted in fig. 9. After an electron is transfered to Q_A, this cofactor moves away from H_L, towards Fe_1 and Q_B, the next electron acceptor. Upon electron transfer the center–center distance

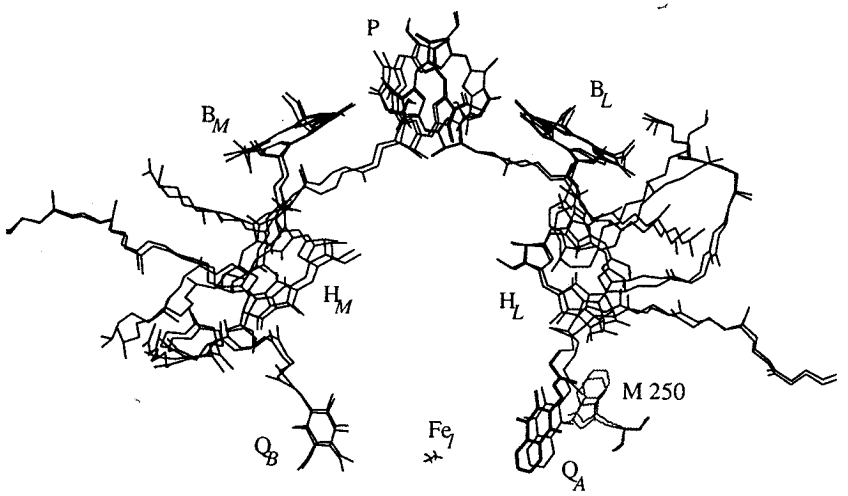

Fig. 9. Superposition of structures of cofactors before and after the electron transfer $H_L \rightarrow Q_A$ at 300 K; both structures were averaged over 0.5 ps. A significant shift of Q_A (bold) as result of the electron transfer can be seen. The transfer-induced motion of residue M250 (grey), a tryptophan, is also shown.

between H_L and Q_A increases by 0.68 Å at 300 K and by 0.4 Å at 80 K, whereas the distance Q_A–Fe_I shrinks by about 0.2 Å. According to eq. (47) below, the altered distances decrease the electronic coupling V between H_L and Q_A by about 50% and increase the coupling between Q_A and Q_B by 30%, i.e., the changed couplings accelerate the forward-transfer $Q_A \rightarrow Q_B$ and slow down the competing back-transfer $Q_A \rightarrow H_L$. Considering the fact that the rates of the forward and the backward transfer are of the same order of magnitude (see fig. 1), the structural rearrangements of the chromophores may contribute to a high overall quantum yield.

As shown in fig. 10, for the electron transfer $H_L \rightarrow Q_A$ the energy difference $\Delta E_{MD}(t)$ between the reactant state $P_S^+ H_L^- Q_A$ and the product state $P_S^+ H_L Q_A^-$ before and after transfer displays very much the same features as the transfer $P_S \rightarrow H_L$: fluctuations around a mean value $\langle \Delta E_{MD} \rangle_R$ before transfer, rapid dielectric relaxation following the transfer, and then fluctuations around a new mean value $\langle \Delta E_{MD} \rangle_P$. The solvation energy $\Delta\Delta E$ for this reaction is greater by almost a factor of two than $\Delta\Delta E$ for the transfer $P_S \rightarrow H_L$. This implies that the protein contribution to the reorganization energy $\lambda_{prot} \approx 5$ kcal/mol (eq. (9), $\epsilon = 2$) is greater for the transfer $H_L \rightarrow Q_A$ than for the transfer $P_S \rightarrow H_L$. The corresponding value for ϵ as defined in eq. (10) for $H_L \rightarrow Q_A$ at 300 K is 14.1 kcal/mol. The decrease of $\langle \Delta E_{MD} \rangle_R$ and $\langle \Delta E_{MD} \rangle_P$ due to a lowering of the temperature is significantly larger than for the transfer $P_S \rightarrow H_L$.

As for the electron transfer $P_S \rightarrow H_L$, the Fourier spectra before and after the transfer $H_L \rightarrow Q_A$ do not differ significantly from each other (see figs. 11, 12) and, as before, the amplitudes of the spectra decrease by a factor of two upon a lowering of the temperature from 300 to 80 K. But in contrast to the Fourier spectra for the transfer $P_S \rightarrow H_L$, the frequency composition of these spectra exhibit a significant temperature dependence. Comparison of figs. 11 and 12 show that the 300 K spectra for the transfer $H_L \rightarrow Q_A$ consist of a band of frequencies which is slightly broader than for the 80 K spectra.

4.5. Rate of electron transfer $P_S \rightarrow H_L$

In this section we present the rates for the electron transfer $P_S \rightarrow H_L$ resulting from the two descriptions outlined in sections 3.1 and 3.2: $k_{cl}^{MD}(\epsilon)$ from the two-state model based on $\Delta E_{MD}(t)$ and $k_{cl}^{ST}(\epsilon)$ from the description involving a stochastic model.

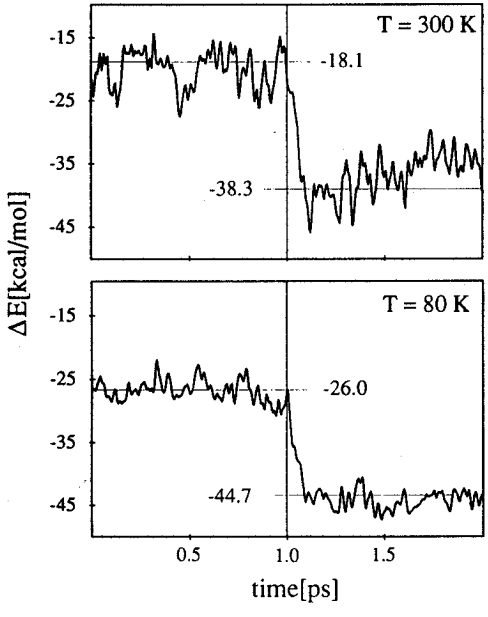

Fig. 10. $\Delta E_{MD}(t)$ for the electron transfer $H_L \rightarrow Q_A$ at 300 and 80 K. At $t = 1.0$ ps an electron was transfered. The mean values were averaged over a 10 ps time span before and over 5 ps after the transfer.

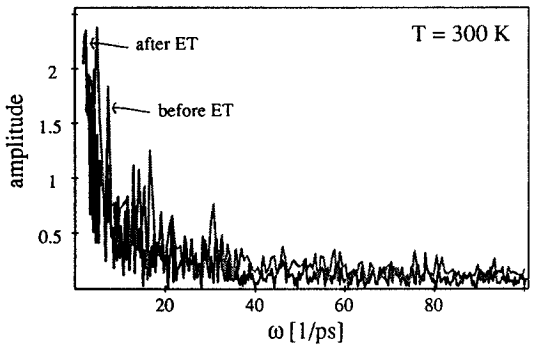

Fig. 11. Fourier spectra of $\Delta E_{MD}(t)$ before and after the electron transfer $H_L \rightarrow Q_A$ calculated for a 5 ps simulation at $T = 300$ K.

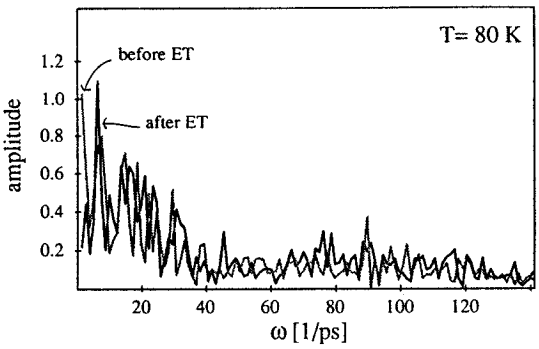

Fig. 12. Fourier spectra of $\Delta E_{MD}(t)$ before and after the electron transfer $H_L \rightarrow Q_A$ calculated for a 5 ps simulation at $T = 80$ K.

4.5.1. The rates k_{cl}^{MD}

The rates $k_{cl}^{MD}(\epsilon)$ were evaluated by solving numerically eqs. (17, 19) for time steps $\Delta t = 5$ fs and piecewise constant $\Delta E_{MD}(t)$. The time series $\Delta E_{MD}(t_j), j = 1, 2, \ldots$ has been based on MD simulations at 300 and at 80 K. We averaged results over five time series, each 5 ps long.

The parameters V and τ which enter the Liouville equation (15) have been chosen as follows. For V we assumed

$$V = V_0 \, e^{-\alpha R_{DA}}, \quad \alpha = 1.4 \, \text{Å}^{-1}, \tag{47}$$

a spatial dependence which had been suggested in refs. [57,47]. The value R_{DA} is the average center–center distance between P_S and H_L and has been determined for phase $P_S H_L Q_A$ of the simulation to be $R_{DA} = 17.8$ Å. For V_0 we assumed a value $V_0/\hbar \approx 217$ fs^{-1} which resulted in $V/\hbar = 5$ ps^{-1}, the value employed in ref. [15]. Note that the value $V_0/\hbar$ does not relate to any direct observable since the edge–edge distance determines $V(r)$. We assumed a life time $\tau = 5$ ps, a value which is considerably longer than the simulated dielectric relaxation time (response time to transfer) which measures 0.05 ps. The values V and τ were adjusted to obtain maximal values of $k_{cl}^{MD}(\epsilon)$ of (3 ps)$^{-1}$, i.e., the value observed for the transfer $P_S \rightarrow H_L$. We like to emphasize, however, that otherwise the values of V and τ are immaterial for the subsequent discussions.

The rates resulting from our simulations are presented in fig. 13. The main result of our calculations is that the fluctuations of $\Delta E_{MD}(t)$ induce a very broad ϵ-dependence of $k_{cl}^{MD}(\epsilon)$. In fact, the electron transfer rate k_{cl}^{MD} is approximately constant over the range 14 to 22 kcal/mol at 300 K, over the range 16 to 23 kcal/mol at 80 K, and decreases rapidly to zero for values of ϵ moving away from these intervals. The $k_{cl}^{MD}(\epsilon)$ curves are centered around the peaks of the distributions $\tilde{p}_0(\Delta E)$ shown in fig. 7 which explains the shift of the rate curves at 300 and 80 K relative to each other by about 2 kcal/mol.

The rates $k_{cl}^{MD}(\epsilon)$ depicted in fig. 13 constitute a main result of this paper. The rates presented have been averaged over five simulations, each 5 ps long. One would expect that further averaging alters to some extent the ϵ-dependence of k_{cl}^{MD} depicted in fig. 13. The ϵ-dependence of k_{cl}^{MD} is similar to the ΔG_0-dependence of transfer rates in the Marcus theory [33,34] and other theories of electron transfer (see ref. [18]), in particular, the dependence shows an inverted region, i.e., a decrease both for high and low ϵ values. The ϵ-dependence of $k_{cl}^{MD}(\epsilon)$ implies that electron transfer rates in the photosynthetic reaction center are insensitive to alterations of the redox energies of respective chromophores over a range of about 15 kcal/mol.

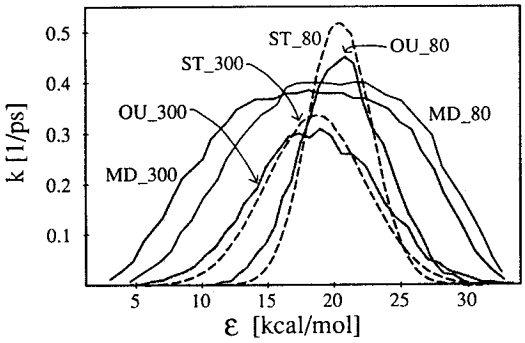

Fig. 13. Electron transfer rates $k_{el}(\epsilon)$ at 300 and at 80 K as a function of the energy ϵ "exchanged" with the quantum-mechanical degrees of freedom. One set of rates k_{el}^{MD} denoted by MD_300 and MD_80 has been evaluated using in the two-state model $\Delta E_{MD}(t)$ and averaging over five runs (solid lines); a second set of k_{el}^{OU} rates denoted by OU_300 and OU_80 has been evaluated similarly, but using in the two-state model $\Delta E_{OU}(t)$ values generated according to an Ornstein–Uhlenbeck process (grey lines); a third set of rates k_{el}^{ST} denoted by ST_300 and ST_80 has been calculated according to the stochastic model in section (3.2) (dashed lines).

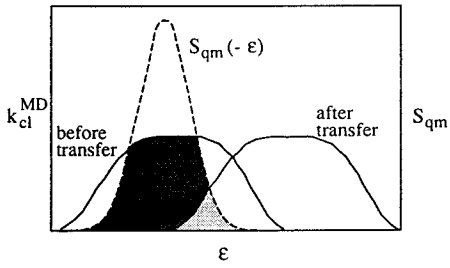

Fig. 14. Schematic presentation of the effect of the dielectric response on the electron transfer rate as described by eq. (12). Before transfer $\mathcal{S}_{qm}(-\epsilon)$ (dashed) and $k_{el}^{MD}(\epsilon)$ overlap well; the sum of the dark-shaded area and the light-shaded area indicates the value of the forward transfer rate. After electron transfer the overlap of $\mathcal{S}_{qm}(-\epsilon)$ and $k_{el}^{MD}(\epsilon)$ is small; the light-shaded area indicates the smaller value of the rate of back transfer.

Shifts of the distribution $\tilde{p}_0(\Delta E)$ resulting through dielectric relaxation after electron transfer (as depicted in fig. 7) cause the $k_{el}^{MD}(\epsilon)$ curves to shift relative to ϵ by the same amount; i.e., dielectric relaxation causes the peak of $k_{el}^{MD}(\epsilon)$ to shift by 10 to 12 kcal/mol after electron transfer. If one assumes that the electron transfer is optimized, i.e., $\mathcal{S}_{qm}(-\epsilon)$ in eq. (12) overlaps well with $k_{el}^{MD}(\epsilon)$, and that $\mathcal{S}_{qm}(-\epsilon)$ is not changed significantly by the electron transfer, the shifted $k_{el}^{MD}(\epsilon)$ may not overlap well with $\mathcal{S}_{qm}(-\epsilon)$. This behavior, presented schematically in fig. 14, provides a mechanism which slows down the rate of backward transfer relative to the rate of forward transfer. The shift by $\epsilon_0 = 11.7$ kcal/mol corresponds to the stabilization of the product state $P^+H_L^-Q_A$ below the state $P^*H_LQ_A$. The value 6 kcal/mol observed for this stabilization includes intramolecular electronic contributions as well as protein contributions.

Fig. 14 can explain also why some rates are more sensitive to alterations of redox energies than others; the dependence on redox energies is different if $\mathcal{S}_{qm}(-\epsilon)$ overlaps in the center of $k_{el}^{MD}(\epsilon)$ or at the edge of $k_{el}^{MD}(\epsilon)$. Accordingly, one can rationalize, in principle, the changes of transfer rates for $P_S \rightarrow H_L$, $H_L \rightarrow Q_A$, and $H_L \rightarrow P_S$ in the genetically engineered reaction center in ref. [17].

4.5.2. The rates k_{el}^{ST}

To investigate which properties of $\Delta E_{MD}(t)$ are essential determinants for the ϵ-dependence of $k_{el}^{MD}(\epsilon)$ we evaluated the electron transfer rates according to the simple stochastic model introduced in section 3.2. This model accounts for the distribution $\tilde{p}_0(\Delta E)$ in fig. 7. Matching of the Gaussian distributions yields σ-values of 5 kcal/mol at 300 K, 3.5 kcal/mol at 80 K, and $\langle \Delta E_{MD} \rangle$ values of 18.3 kcal/mol at 300 K, 20.3 kcal/mol at 80 K.

The stochastic model also accounts for the mean relaxation time of the correlation function in eq. (23). This correlation function is presented in fig. 15. The match of a mono-exponential decay at both temperatures, i.e.,

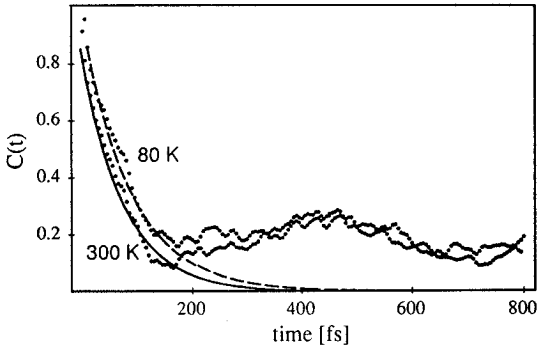

Fig. 15. Comparison of the autocorrelation function $C(t)$, defined in eq. (23) evaluated from $\Delta E_{MD}(t)$ and mono-exponential fits at 300 and 80 K. The mono-exponential fits yield the mean relaxation times.

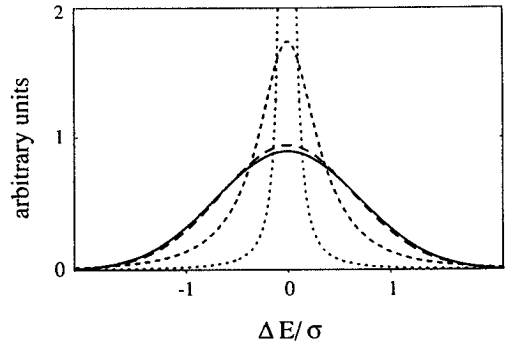

Fig. 16. Comparison of the static distribution $\tilde{p}_0(\Delta E)$ and the line shape function $\mathscr{I}(\Delta E)$ for various values of $\rho = D\hbar/\sigma^3$: (——) $\tilde{p}_0(\Delta E)$, (– – –) $\mathscr{I}(\Delta E)$ for $\rho = 0.07$, (– – –) same for $\rho = 0.7$, (····) same for $\rho = 7$. The line shape function $\mathscr{I}(\Delta E)$ has been evaluated as described in ref. [58].

300 and 80 K, results in $\tau \approx 0.1$ ps, which according to eq. (23) corresponds to $D/\sigma^2 = 10\ \text{ps}^{-1}$. Fig. 15 shows that the match at times $t > 200$ fs is rather poor. The deviation is indicative of contributions to $C(t)$ with slower relaxation times. The determination of $k_{cl}^{MD}(\epsilon)$ according to eqs. (20–29) requires the numerical evaluation of the line shape function $\mathscr{I}(\Delta E')$ defined in eq. (29). A method for the evaluation of $\mathscr{I}(\Delta E')$ is presented in appendix A.

The rates $k_{cl}^{ST}(\epsilon)$ at 300 and at 80 K are depicted in fig. 13. The ϵ-dependence of $k_{cl}^{ST}(\epsilon)$ is bell-shaped, peaked at the maximum of the distributions $\tilde{p}_0(\Delta E)$. The shape of $k_{cl}^{ST}(\epsilon)$ is essentially identical to the line shape function $\mathscr{I}(\Delta E')$ since in the convolution integral (34) the width of $\hat{k}(\epsilon - \Delta E')$ is of the order V, i.e., measures only about 0.1 kcal/mol.

We have derived above that the shape of $\mathscr{I}(\Delta E)$ and, hence, of $k_{cl}^{ST}(\epsilon)$ is controlled by the parameter ρ defined in eq. (36). The case of static disorder in ΔE is described by $\rho = 0$, slow fluctuations $\Delta E(t)$ correspond to $\rho \ll 1$, and fast fluctuations to $\rho \gg 1$. In fig. 16 we compare line shape functions for vanishing ρ (static disorder), and for ρ values 0.07, 0.7, 7. Fig. 16 demonstrates that, for small ρ values, $\mathscr{I}(\Delta E)$ matches closely $\tilde{p}_0(\Delta E)$, a discernable, but small deviation developing for $\rho = 0.07$. A value $\rho = 0.7$ yields a distinct deviation from $\tilde{p}_0(\Delta E)$ and, in the case $\rho = 7$, the motional narrowing limit is being approached. The ρ value corresponding to the simulations at 300 K is 0.03. According to fig. 16 one can expect in the case of simulated $\Delta E(t)$ values that $\mathscr{I}(\Delta E)$ is essentially identical to $\tilde{p}_0(\Delta E)$. Since the ϵ-dependence of the rates $k_{cl}^{ST}(\epsilon)$ actually matches then $\tilde{p}_0(\Delta E)$ closely, according to the derivation provided in section 3.3 the rates $k_{cl}^{ST}(\epsilon)$ reproduce then the same ΔG_0-dependence as predicted by the Marcus theory of electron transfer. This implies the motional narrowing effects due to protein dynamics are negligible. This finding provides strong support for the conventional second-order perturbation treatment of electron transfer in proteins.

The rates $k_{cl}^{ST}(\epsilon)$ do not display a broad plateau like the rates $k_{cl}^{MD}(\epsilon)$; their width is only half of the width of the rates $k_{cl}^{MD}(\epsilon)$. This difference between the rates $k_{cl}^{MD}(\epsilon)$ and $k_{cl}^{ST}(\epsilon)$ is due to the fact that the stochastic process (Ornstein–Uhlenbeck process) is too idealized, being based only on time-averaged quantities of $\Delta E_{MD}(t)$. In fact, a comparision of the energy autocorrelation function $C(t)$ in fig. 15 with velocity autocorrelation functions of single atoms in ref. [27] suggests that $\Delta E(t)$ is made up of single mode contributions which have a broad low-frequency Fourier spectrum and a high-frequency spectrum characterized by a few sharp lines. An average over such a spectrum would yield spectra as in figs. 8, 11 and 12, namely, a dominant low-frequency band and small, but essential contributions at high frequencies. We suggest that, according to the mechanism outlined in section 3, high-frequency contributions to $\Delta E(t)$ are the origin of the deviation between $k_{cl}^{MD}(\epsilon)$ and $k_{cl}^{ST}(\epsilon)$.

4.5.3. The rates k_{cl}^{OU}

In order to test in how far the discrepancy between $k_{cl}^{MD}(\epsilon)$ and $k_{cl}^{ST}(\epsilon)$ might not be due to errors in our analysis of $\Delta E_{MD}(t)$, we generated random sequences $\Delta E_{OU}(t)$ according to an Ornstein–Uhlenbeck process which reproduces distribution (21) and autocorrelation function (22) (we assumed the same parameters $\langle \Delta E_{MD} \rangle$, σ and D as for the evaluation of k_{cl}^{ST}). The generation of the random sequence $\Delta E_{OU}(t)$ is described in appendix B. We then replaced $\Delta E_{MD}(t)$ by $\Delta E_{OU}(t)$ in evaluating the electron transfer rate as described in section 3.1. The rates obtained are denoted by $k_{cl}^{OU}(\epsilon)$.

The rates $k_{cl}^{OU}(\epsilon)$, averaged over ten sequences 5 ps long of $\Delta E_{OU}(t)$, are displayed in fig. 13. The rates $k_{cl}^{OU}(\epsilon)$ are in good agreement with the rate $k_{cl}^{ST}(\epsilon)$ indicating that two possible errors in our analysis are insignificant: (i) an error due to the approximations in the line shape approach as discussed in ref. [39], (ii) an error due to the use of discrete time steps in calculating rates by the two-state model which, in principle, could introduce spurious frequency behavior.

The difference in width between $k_{cl}^{MD}(\epsilon)$ and $k_{cl}^{OU}(\epsilon)$, therefore, should be due to the broader frequency spectrum of $\Delta E_{MD}(t)$ compared to the frequency spectrum of $\Delta E_{OU}(t)$. In fig. 17 the frequency spectrum $\Delta \hat{E}_{OU}(\omega)$ of $\Delta E_{OU}(t)$ is presented. This spectrum, when averaged over a large number of Ornstein–Uhlenbeck processes, converges to the Lorentzian $[\omega^2+a^2]^{-1}$ with $a=D/\sigma^2$ (see eq. (22)). The amplitudes of $\Delta \hat{E}_{OU}(\omega)$ in the low-frequency range (1–20 ps^{-1}) are larger than the amplitudes of the spectrum of $\Delta \hat{E}_{MD}(\omega)$ in this range. However, this difference cannot account for the deviation between $k_{cl}^{MD}(\epsilon)$ and $k_{cl}^{ST}(\epsilon)$ ($k_{cl}^{OU}(\epsilon)$). We conclude, therefore, that the broad ϵ-dependence of the electron transfer rates $k_{cl}^{MD}(\epsilon)$ reflects the coupling of higher-frequency vibrations to electron transfer as explained in section 3.3.

The main characteristic of the ϵ-dependence of $k_{cl}^{MD}(\epsilon)$, the wide range of relatively large rate values with only a weak ϵ-dependence, is corroborated by observations reported in refs. [17,18], namely, that redox-energy changes of up to 0.4 eV affect transfer rates in photosynthetic reaction centers only to a small degree. The authors of ref. [18], in fact, needed to include modes with three frequencies to match an expression of the type of eqs. (11, 13, 14) to the observed redox energy dependence of transfer rates. Since one expects a simple Marcus type redox energy dependence for the rate k_{cl}^{ST} the observations reported in ref. [18] may be indicative of the role of higher-frequency vibrations discussed above. In fact, in ref. [18] the authors matched their data through an expression of the type of eq. (11) using higher frequency vibrations represented through $\mathcal{S}_{qm}(\epsilon)$. This contribution provided an additional broadening of the ΔG-dependence of transfer rates required to fit the observations. In this respect the data appear to support the simulations: the rates $k_{cl}^{ST}(\epsilon)$ which represent a classical mechanical behavior of coupling to low medium frequencies appear to have too narrow an energy dependence which, however, is broadened through higher-frequency medium vibrations and librations, as exhibited through $k_{cl}^{ST}(\epsilon)$ and as explained above. In ref. [25] such broadening had been achieved in a stochastic Marcus model through introduction of a "wide reaction window" which corresponds to employing in eq. (11) a broad $\mathcal{S}_{qm}(\epsilon)$. It appears then that one of the main results of this paper, the broad ϵ-dependence of k_{cl}^{MD}, is corroborated by the approaches assumed in refs. [18,25].

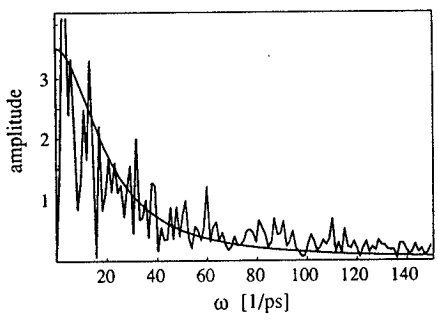

Fig. 17. Fourier spectrum of $\Delta E_{OU}(t)$ obtained from the Ornstein–Uhlenbeck process, calculated for a 5 ps series and with 300 K parameters. Also shown is a fit to a Lorentzian.

5. Summary

Understanding how organic media control redox processes remains a major challenge. The challenge involves on the scale of a large biopolymer one of the most fundamental questions of chemistry: how do electronic and nuclear degrees of freedom cooperate to transform an electronic state and nuclear configuration into another electronic state and nuclear configuration. Photosynthetic reaction centers with an easily controlled, namely light-induced, electron transfer chain which at the same time is observable well by spectroscopic means, has made possible some of the most important research in this respect. These protein complexes are good laboratories for the study of electron transfer in structurally well defined circumstances, they also add a new challenge: the reaction centers contain 12 electron donor–acceptor groups in a geometrical setting (see fig. 1 presenting 8 of the chromophores) which does not make it apparent why the conducted electrons follows always one and the same path through the set of chromophores in fig. 1. For example, we do not yet have a satisfactory answer to the question why the electrons with essentially 100% certainty go to H_L rather than to H_M, a group located in a manner nearly symmetric to that of H_L. Along which path does the electron tunnel to H_L? Which role do the nuclear degrees of freedom play at this instance, the one described in refs. [30,31]? Also a question in need of further investigation is why the electron transfers do not slow down significantly (actually in some cases increase) as temperature is lowered (see ref. [26] and references cited therein).

Above we have attempted to address some of these issues using the fact that the availability of the structure of the photosynthetic reaction centers provides the opportunity to guide research on redox processes by MD simulations. These simulations, at worst, allow one to "play" with concrete molecular models to stimulate one's phantasy and, at best, allow one to obtain solid information on the behavior of the nuclear degrees of freedom in the classical limit. The work reported is only a beginning, a difficult one due to the fact that the photosynthetic reaction centers investigated are very large, such that current computational technologies make simulations of the complete system, or large enough sections of it, difficult. The advent of massively parallel computers actually has improved this situation [59,60] and, most likely, simulations of photosynthetic reaction centers and of other redox proteins will proliferate after such computers become more widely available.

The simulations presented above describe the nuclear degrees of freedom classically, quantum mechanical simulations of biopolymers being currently out of sight. Also, the effect of the electron on the nuclear degrees of freedom through the considerable change of chromophore charge distributions accompanying transfer has been described in a very arbitrary manner. Nevertheless, the shift of a complete electron charge at an arbitrary instance in time revealed a very rapid dielectric response of the protein, a feature which certainly relates to the ability of the nuclear degrees of freedom to interact effectively with the electron during the tunneling event. Since neither the quantum nature of nuclear motion nor the electron tunneling process can be directly described through simulations, one needs to resort to a model which entails the essentials of electron–nuclear coupling and is simple enough to be amenable to a quantum mechanical analysis. The spin–boson model described in section 1 and confirmed to some degree by the results of the MD simulations, as presented in section 4, qualifies in this respect. Further investigations should be carried out in the framework of the spin–boson model rather than in the framework of cumbersome MD simulations. For example, the low-temperature behavior of electron transfer in reaction centers can be studied in the confines of the spin–boson model following ref. [28]. We have recently completed such investigation [26].

Acknowledgement

We like to thank J. Deisenhofer for kindly providing us with the X-ray structure of the reaction center of *Rps. viridis*, H. Treutlein for an equilibrated 300 K conformation of the reaction center, A. Brünger for making upgraded versions of the program X-Plor available to us, B. Puetz for providing fig. 16, and R. Bittl for helpful discussions regarding the line shape approach. We are grateful to A. Legget for pointing us to the spin–boson

problem. This research has been carried out in the Center for Parallel Computation in Molecular Dynamics funded by the National Institute of Health (Grant 1P41RR05969*01). Computation time was granted to us by the National Center of Supercomputer Applications supported by the National Science Foundation.

Appendix A. Numerical evaluation of line shape function

We evaluate the line shape function through expansion in terms of the right ($\langle u|m\rangle$) and left ($\langle\tilde{n}|u\rangle$) eigenfunctions of the operator $\mathscr{L}=D\partial_u p_0(u)\partial_u[p_0(u)]^{-1}$ given in the Fokker–Planck equation (20)

$$\langle u|n\rangle=\frac{1}{\sqrt{\pi}}\frac{2^{-n}}{n!}e^{-u^2}H_n(u),\quad \langle\tilde{m}|u\rangle=H_m(u)\,, \tag{A.1}$$

where H_m denotes the Hermite polynomial. We assume in the following $\sigma=1$, i.e., measure u in units of σ and D in units of σ^{-2}. It holds [51]

$$\langle\tilde{m}|n\rangle=\frac{1}{\sqrt{\pi}}\frac{2^{-n}}{n!}\int_{-\infty}^{\infty}du\,H_m(u)e^{-u^2}H_n(u)=\delta_{mn}\,, \tag{A.2}$$

i.e. $\langle\tilde{m}|u\rangle$ and $\langle u|n\rangle$ form a bi-orthogonal system. One can show that this system is complete, i.e., it spans the function space $\{f(u),\ u\in[-\infty,\infty],\ f\text{continuous}\}$. The eigenvalues of $\mathscr{L}$ follow from the property [51]

$$\mathscr{L}|n\rangle=-2mD|n\rangle,\quad \langle\tilde{m}|\mathscr{L}^{\dagger}=-2mD\langle\tilde{m}|\,. \tag{A.3}$$

According to ref. [51] holds

$$\langle u|n+1\rangle=2u\langle u|n\rangle-2n\langle u|n-1\rangle,\quad \langle\tilde{m}|u|n\rangle=\tfrac{1}{2}\delta_{mn+1}+n\delta_{mn-1}\,. \tag{A.4}$$

From this and eq. (A.3) we obtain

$$\langle\tilde{m}|i(u-u')-\mathscr{L}|n\rangle=(2nD-iu')\delta_{mn}+\frac{i}{2}\delta_{mn+1}+in\delta_{mn-1}\equiv B_{mn}(u')\,, \tag{A.5}$$

where **B** is an infinite-dimensional, tri-diagonal matrix. Obviously

$$\langle u|0\rangle=p_0(u),\quad \langle\tilde{0}|u\rangle=1\,. \tag{A.6}$$

Eq. (29) yields then

$$\mathscr{I}=\frac{1}{\pi}\mathrm{Re}[B^{-1}(u')]_{00}\,. \tag{A.7}$$

In order to evaluate $[B^{-1}(u')]_{00}$ we start from

$$(1\,0\ldots)B^{-1}(u')\begin{pmatrix}1\\0\\\vdots\end{pmatrix}=[B^{-1}(u')]_{00}\,, \tag{A.8}$$

which can be written as

$$\begin{pmatrix}1\\0\\\vdots\end{pmatrix}=B(u')\begin{pmatrix}y_0\\y_1\\\vdots\end{pmatrix},\quad y_0=[B^{-1}(u')]_{00}\,. \tag{A.9}$$

The latter equation together with eq. (A.5) can be written in matrix notation

$$\begin{pmatrix} -iu' & i/2 & 0 & \dots & & & \\ i & 2D-iu' & i/2 & 0 & \dots & & \\ 0 & 2i & 4D-iu' & i/2 & 0 & \dots & \\ \vdots & \ddots & \ddots & \ddots & \ddots & \ddots & \dots \\ 0 & \dots & 0 & 2ni & 2nD-iu' & i/2 & \dots \\ \vdots & \vdots & \dots & \ddots & \ddots & \ddots & \ddots \end{pmatrix} \begin{pmatrix} y_0 \\ y_1 \\ y_2 \\ \vdots \\ y_n \\ \vdots \end{pmatrix} = \begin{pmatrix} 1 \\ 0 \\ 0 \\ \vdots \\ 0 \\ \vdots \end{pmatrix} \tag{A.10}$$

For the numerical solution a finite dimension $N=2000$ is assumed for the matrix **B**.

The ensuing problem has been discussed in ref. [61], albeit for a real matrix **B**. The use of a finite-dimensional matrix **B** can only be justified for $u' \ll N$.

Appendix B. Simulation of Ornstein–Uhlenbeck process

The Ornstein-Uhlenbeck process [53,54] is defined by the probabilities [$u=\Delta E(t)$]

$$p(u)=\frac{1}{\sqrt{2\pi\sigma}}\exp[-(u-\langle u\rangle)^2/2\sigma^2]\,, \tag{B.1}$$

$$p[(u(t_1)\,|\,(u(t_0)]=\frac{1}{\sqrt{2\pi s}}\exp[-[u(t_1)-u(t_0)e^{-D\Delta t/\sigma^2}]^2/2s]\,, \tag{B.2}$$

where $\Delta t=t_1-t_0$, $s=(\sigma^2/2)(1-\exp[-2D\Delta t/\sigma^2])$. $p[u(t_1)\,|\,u(t_0)]$ denotes a conditional probability. $\langle u\rangle$, σ and D are defined by eqs. (21, 22) based on the $\Delta E_{\mathrm{MD}}(t)$ values of the MD simulations and were given the same values as used for the evaluation of $k_{\mathrm{el}}^{\mathrm{ST}}(\epsilon)$.

To generate a sequence of $u(t)$-values with the properties given in eq. (B.2), we produced two different sets of Gaussian-distributed random numbers as described in ref. [61]; one set denoted by U has the same width σ^2, and the other set denoted by W has a width $s=\frac{1}{2}\sigma^2(1-\exp[-4D\Delta t/\sigma^2])$, $\Delta t=5$ fs. The time series of $u(t_n)$ was then generated according to $u(t_{n+1})=w_n+u(t_n)\exp[2D\Delta t/\sigma^2]$, where $u(t_n)$ is a value from the set U and w_n is a value from the set W.

References

[1] C. Kirmaier and D. Holten, Photosynthesis Res. 13 (1987) 225–260.
[2] W.W. Parson, in: New Comprehensive Biochemistry: Photosynthesis, ed. J. Amesz (Elsevier, Amsterdam, 1987) pp. 43–61.
[3] S.G. Boxer, R.A. Goldstein, D.J. Lockhart, T.R. Middendorf and L. Takiff, J. Phys. Chem. 93 (1989) 8280.
[4] J.P. Allen, G. Feher, T.O. Yeates, H. Komiya and D.C. Rees, Proc. Natl. Acad. Sci. USA 84 (1987) 5730.
[5] J.P. Allen, G. Feher, T.O. Yeates, H. Komiya and D.C. Rees, Proc. Natl. Acad. Sci. USA 84 (1987) 6162.
[6] D.E. Budil et al., Advan. Rev. Phys. 38 (1987) 561.
[7] J. Deisenhofer, O. Epp, K. Miki, R. Huber and H. Michel, J. Mol. Biol. 180 (1984) 385.
[8] J. Deisenhofer, O. Epp, K. Miki, R. Huber and H. Michel, Nature 318 (1985) 618.
[9] J. Deisenhofer and H. Michel, Science 245 (1989) 1463.
[10] J. Breton, J.L. Martin, A. Migus, A. Antonetti and A. Orszag, Proc. Natl. Acad. Sci. USA 83 (1986) 5121.
[11] R.A. Marcus, Chem. Phys. Letters 133 (1987) 471.
[12] Holzapfel et al., Proc. Natl. Acad. Sci. USA 87 (1990) 5168.
[13] C.A. Wraight and R.K. Clayton, Biochim. Biophys. Acta 333 (1974) 246.
[14] H. Treutlein, K. Schulten, J. Deisenhofer, H. Michel, A. Brünger and M. Karplus, Proc. Natl. Acad. Sci. USA, in press.
[15] G.R. Fleming, J.L. Martin and J. Breton, Nature 333 (1988) 190.

[16] C. Kirmaier and D. Holten, in: The Photosynthetic Bacterial Reaction Center: Structure and Dynamics, eds. J. Breton and A. Vermeglio (Plenum Press, London, 1988) pp. 219–228.
[17] C. Kirmaier, D. Gaul, R. DeBrey, D. Holten and C. Schenck, Science 251 (1991) 922.
[18] M.R. Gunner and P.L. Dutton, J. Am. Chem. Soc. 111 (1989) 3400.
[19] S. Creighton, J.-K. Hwang, A. Warshel, W.W. Parson and J. Norris, Biochemistry 27 (1988) 774.
[20] A. Warshel, Z.T. Chu and W.W. Parson, Science 246 (1989) 112.
[21] R.A. Kuharsky, J.S. Bader, D. Chandler, M. Sprik, M.L. Klein and R.W. Impey, J. Chem. Phys. 89 (1988) 3248.
[22] C. Zheng, J.A. McCammon and P.G. Wolynes, Proc. Natl. Acad. Sci. USA 86 (1989) 6441.
[23] G. van der Zwan and J.T. Hynes, J. Phys. Chem. 85 (1985) 4181.
[24] M. Maroncelli and G.R. Fleming, J. Chem. Phys. 86 (1987) 6221.
[25] H. Sumi and R.A. Marcus, J. Chem. Phys. 84 (1986) 4894.
[26] D. Xu and K. Schulten, submitted to Chem. Phys.
[27] W. Nadler, K. Schulten, A. Brünger and M. Karplus, Proc. Natl. Acad. Sci. USA 84 (1987) 7933.
[28] A.J. Leggett, S. Chakravarty, A.T. Dorsey, M.P.A. Fisher, A. Garg and W. Zwerger, Rev. Mod. Phys. 59 (1987) 2.
[29] J.N. Onuchic, J. Chem. Phys. 86 (1987) 3925.
[30] G.A. Voth, D. Chandler and W.H. Miller, J. Chem. Phys. 91 (1989) 7749.
[31] J.S. Bader, R.A. Kuharsky and D. Chandler, J. Chem. Phys. 93 (1990) 230.
[32] L. Onsager, Can. J. Chem. 55 (1977) 1819.
[33] R. Marcus, J. Chem. Phys. 24 (1956) 966.
[34] R. Marcus, J. Chem. Phys. 24 (1956) 979.
[35] W. Nadler and R.A. Marcus, J. Chem. Phys. 86 (1987) 3906.
[36] M. Nonella and K. Schulten, J. Phys. Chem. 95 (1991) 2059.
[37] A. Yoshimori and T. Kakitani, J. Chem. Phys. 93 (1990) 5140.
[38] R. Kubo, Advan. Chem. Phys. 15 (1969) 101.
[39] R. Bittl and K. Schulten, J. Chem. Phys. 90 (1989) 1794.
[40] A.T. Brünger, in: Crystallographic Computing 4: Techniques and New Technologies, eds. N.W. Isaacs and M.R. Taylor (Clarendon Press, Oxford, 1988).
[41] B.R. Brooks, R.E. Bruccoleri, B.D. Olafson, D.J. States, S. Swaminathan and M. Karplus, J. Comput. Chem. 4 (1983) 187.
[42] M. Berkowitz and J.A. McCammon, Chem. Phys. Letters 90 (1982) 215.
[43] C.L. Brooks, A. Brünger and M. Karplus, Biopolymers 24 (1985) 843.
[44] M. Tesch and K. Schulten, Chem. Phys. Letters 169 (1990) 97.
[45] W.F. van Gunsteren and H.J.C. Berendsen, Mol. Phys. 34 (1977) 1311.
[46] M. Plato, F. Lendzian, W. Lubitz, E. Tränkle and K. Möbius, in: The Photosynthetic Bacterial Reaction Center: Structure and Dynamics, eds. J. Breton and A. Vermeglio (Plenum Press, London, 1988) p. 379.
[47] R.A. Marcus and N. Sutin, Biochim. Biophys. Acta 811 (1985) 265.
[48] J. Ulstrup, Charge Transfer Processes in Condensed Media (Springer, Berlin, 1979).
[49] D. DeVault, Quantum-mechanical Tunneling in Biological Systems (Cambridge Univ. Press, Cambridge, 1984).
[50] J.J. Markham, Rev. Mod. Phys. 31 (1959) 956.
[51] M. Abramowitz and I.A. Stegun, Handbook of Mathematical functions (Dover, New York, 1972).
[52] J. Jortner, J. Chem. Phys. 64 (1976) 4860.
[53] G.E. Uhlenbeck and L.S. Ornstein, Phys. Rev. 36 (1930) 823.
[54] S. Chandrasekhar, Rev. Mod. Phys. 15 (1943) 1.
[55] C.P. Slichter, in: Principles of Magnetic Resonance, 3rd Ed. (Springer, Berlin, 1990).
[56] IMSL Inc., Bellaire Blvd., Houston TX 77036. ISML library reference manual, 8 edition, 1980.
[57] J.R. Miller, in: Antennas and Reaction Centers of Photosynthetic Bacteria – Structure, Interaction and Dynamics, ed. M. Michel-Beyerle (Springer, Berlin, 1985) pp. 234–241.
[58] B. Puetz, D. Barsky and K. Schulten, J. Magn. Reson., in press.
[59] H. Heller, H. Grubmüller and K. Schulten, Mol. Sim. 5 (1990) 133.
[60] A. Windemuth and K. Schulten, Mol. Sim. 6 (1991) 353.
[61] W.H. Press, B.P. Flannery, S.A. Teukolsky and W.T. Vetterling, Numerical Recipes in C (Cambridge Univ. Press, Cambridge, 1988).